

# Quantum Information Scrambling in Graphene Flakes

A Thesis

submitted to

Indian Institute of Science Education and Research Pune

in partial fulfillment of the requirements for the

BS-MS Dual Degree Programme

by

Devjyoti Tripathy



Indian Institute of Science Education and Research Pune

Dr. Homi Bhabha Road,  
Pashan, Pune 411008, INDIA.

April, 2023

Supervisor: Dr. Sebastian Deffner


© Devjyoti Tripathy 2023

All rights reserved



# Certificate

This is to certify that this dissertation entitled Quantum Information Scrambling in Graphene Flake towards the partial fulfilment of the BS-MS dual degree programme at the Indian Institute of Science Education and Research, Pune represents study/work carried out by Devjyoti Tripathy at Indian Institute of Science Education and Research under the supervision of Dr. Sebastian Deffner, Associate Professor, Department of Physics, University of Maryland, Baltimore County (UMBC), during the academic year 2022-2023.

A handwritten signature in black ink, reading "Sebastian Deffner". The signature is fluid and cursive, with the first name "Sebastian" and the last name "Deffner" clearly distinguishable.

Dr. Sebastian Deffner

Committee:

Dr. Sebastian Deffner

Dr. Bijay Kumar Agarwalla



This thesis is dedicated to the quote

—“ **Inherited Will, The Destiny Of Age, The Dreams Of Its People. As Long As People Continue To Pursue The Meaning Of Freedom, These Things Will Never Cease!**”

Pirate King Gold D Roger, One Piece



# Declaration

I hereby declare that the matter embodied in the report entitled Quantum Information Scrambling in Graphene Flakes are the results of the work carried out by me at the Department of Physics, Indian Institute of Science Education and Research, Pune, under the supervision of Dr. Sebastian Deffner and the same has not been submitted elsewhere for any other degree.



Devjyoti Tripathy





# Acknowledgments

I would like to thank my supervisor Dr. Sebastian Deffner for his constant guidance and support throughout the duration of the project. I would also like to thank my collaborators Akram Touil (PhD student, University of Maryland Baltimore County) and Dr. Bartłomiej Gardas (Associate professor, Institute of Theoretical and Applied Informatics, Polish Academy of Sciences, Gliwice, Poland) for their invaluable discussions and insight. Lastly, I also thank my family and friends for their continued and unconditional support.



# Abstract

In this thesis, we study quantum information scrambling in the Bose Hubbard model on two dimensional honeycomb lattices. Using Krylov subspace methods, we compute Out-of-time Ordered Correlators (OTOCs) and other information theoretic measures for our model and we find that the system is quantum chaotic at strong couplings. The scrambling dynamics are sensitive to the surroundings of the two local sites chosen for the OTOC and also display an interesting Gaussian to near-exponential behavior similar to that of the decoherence function. We present a master equation by considering a subsystem of the lattice as an open system and leave the exact numerical solution to the master equation for future reference. We also make attempts to relate the quantum work distribution and quantum coherence with information scrambling.



# Contents

<b>Abstract</b>	<b>xi</b>
<b>1 Introduction and Preliminaries</b>	<b>5</b>
1.1 Introduction	5
1.2 OTOCs as indicators of scrambling	7
1.3 Other measures of information scrambling	10
1.4 Bose Hubbard Model and Honeycomb Lattice	11
<b>2 Scrambling, Decoherence and Results</b>	<b>17</b>
2.1 OTOC as a convolution function	17
2.2 Results	19
2.3 Bose Hubbard model as an open system	34
<b>3 Thermodynamics of Scrambling and Concluding Remarks</b>	<b>43</b>
3.1 Work distribution, Coherence and Scrambling	43
3.2 Mutual Information, Scrambling and Open systems	46
<b>4 Conclusion</b>	<b>49</b>
<b>A Exponential of Matrix using Krylov subspace methods</b>	<b>55</b>



# List of Figures

1.1	Understanding OTOC from an operator growth perspective . . . . .	8
1.2	Illustration of Scrambling for various types of thermalisations [32] . . . . .	9
1.3	Phase diagram of Bose Hubbard model [22] . . . . .	12
1.4	Classical and Quantum chaos indicator for the Bose Hubbard model [19] . . . . .	12
1.5	Decay of correlations with distance when $U = 40J$ [14] . . . . .	13
1.6	Decay of correlations with distance when $U = 4J$ [14] . . . . .	14
1.7	Energy band gaps for graphene . . . . .	16
2.1	$ \langle a_1(t)^\dagger a_2^\dagger a_1(t) a_2 \rangle_\psi $ for the one dimensional Bose Hubbard model with $N=6$ , $L=6$ for $U/J = 0.25$ , $ \psi\rangle =  1, 1, 1, 1, 1, 1\rangle$ . . . . .	20
2.2	$ \langle a_1(t)^\dagger a_2^\dagger a_1(t) a_2 \rangle_\psi $ for the one dimensional Bose Hubbard model with $N=6$ , $L=6$ for $U/J=4$ , $ \psi\rangle =  1, 1, 1, 1, 1, 1\rangle$ . . . . .	20
2.3	$ \langle a_1(t)^\dagger a_2^\dagger a_1(t) a_2 \rangle $ for the one dimensional Bose Hubbard model with $N=6$ , $L=6$ for a range of coupling strengths . . . . .	21
2.4	Change in mutual information for the one dimensional Bose Hubbard model with $N=6$ , $L=6$ $\Delta I(A : B)$ over equal partitions A and B for $U/J=4$ . . . . .	22
2.5	Comparison between change in OTOC and change in Mutual Information for the one dimensional Bose Hubbard model with $N=6$ , $L=6$ . . . . .	23
2.6	Tripartite Mutual Information $I_3(A : B : C)$ for the one dimensional Bose Hubbard model with $N=6$ , $L=6$ where A is a reference boson and B,C are partitions of the 6 site lattice . . . . .	24

2.7 Configuration of two dimensional hex lattices for case 1 where OTOCs for all hex lattices match . . . . .	25
2.8 Behavior of OTOCs for the case ( Fig (2.7) ) when all OTOCs agree for the initial state $ \psi\rangle =  1, 1, 1, 1, 1\rangle$ . . . . .	26
2.9 Strip Configuration for the two dimensional hex lattices . . . . .	27
2.10 Behavior of OTOCs for the strip configuration ( Fig (2.9) ) for the initial state $ \psi\rangle =  1, 1, 1, 1, 1\rangle$ . . . . .	27
2.11 Data fit for OTOC of 1 hex strip configuration ( Fig (2.10) ) . . . . .	28
2.12 Data fit for OTOC of 2 hex strip configuration ( Fig (2.10) ) . . . . .	28
2.13 Data fit for OTOC of 3 hex strip configuration ( Fig (2.10) ) . . . . .	29
2.14 Flake configuration for two dimensional hex lattices . . . . .	30
2.15 Behavior of OTOCs for the flake configuration ( Fig (2.14) ) for the initial state $ \psi\rangle =  1, 1, 1, 1, 1\rangle$ . . . . .	30
2.16 Data fit for OTOC of 2 hex flake configuration ( Fig (2.15) ) . . . . .	31
2.17 Data fit for OTOC of 3 hex flake configuration ( Fig (2.15) ) . . . . .	31
2.18 Bath correlation functions for strip configuration . . . . .	40
2.19 Bath correlation functions for flake configuration . . . . .	41



# List of Tables

<a href="#">2.1 Parameters for strip configuration</a>	33
<a href="#">2.2 Parameters for flake configuration</a>	33
<a href="#">2.3 Convolution parameters for strip configuration</a>	33
<a href="#">2.4 Convolution parameters for flake configuration</a>	34



# Chapter 1

## Introduction and Preliminaries

### 1.1 Introduction

Information Scrambling refers to spreading of quantum information and effective loss of local initial information in quantum many body systems. Here, the system becomes memoryless and insensitive to its initial conditions. It seems like an inconsistent idea because of the fact that these are closed quantum systems which obey unitary evolution. It so happens that an initially localised information spreads throughout the system and appears in the non-local degrees of freedom. Information scrambling can be measured using various quantities such as the Out-of-time Ordered Correlator, entanglement entropy, mutual information, tripartite mutual information, dynamics of local observables and others. The notion of scrambling appears in a lot of areas of physics such as thermalization, black hole information paradox, quantum chaos and so on [9, 30, 3, 7, 20, 8, 23]. Information scrambling has been verified experimentally in superconducting quantum processors [33, 15] and in actual quantum systems such as trapped ions and cold atoms [24, 6, 16].

In the context of the famous information paradox, the black hole is treated as a unitary circuit. Alice encodes an initial state within this setup and this information scrambles throughout the quantum circuit. Bob can then decode Alice's initial state and such decoding protocols are inspired from ideas on teleportation through a wormhole [15, 31, 2]. The holographic principle connects certain quantum field theories to gravity theories in one extra dimension [17]. Using this holographic duality, a great deal of understanding about the

quantum nature of black holes has been achieved by studying the properties of their dual strongly interacting quantum systems such as the Sachdev-Ye-Kitaev(SYK) model which is a system of interacting Majorana fermions. [13], [18]

One of the widely used measures of scrambling is the OTOC which has been studied in this thesis. This quantity cannot distinguish between information scrambling and decoherence [31]. The external noise in an experimental setup and decoherence from interacting with the environment also lead to the decay of OTOCs even in the absence of scrambling dynamics. The interplay between scrambling and decoherence was also recently explored using mutual information of open systems. [25]

In this work, we study information scrambling in the Bose Hubbard model on graphene like lattices. It was shown that electrons in graphene exhibit quantum phases which are described by black hole in the dual theory of AdS [4]. The Bose-Hubbard model is known to be dual to gravity theory in AdS [5]. It also shows quantum chaos: exponential decay of the OTOC in one dimensional lattices, eigenvalue spacing distributions, eigenvalue thermalization hypothesis and other such measures [19], [22]. Here, we explore the scrambling effects in Bose Hubbard model in two dimensional graphene geometries using exact diagonalization techniques and build an open system framework to understand scrambling in unitary models as decoherence of information from localised sites treated as open system. This thesis is presented in four broad parts.

1. The first part consists of the next four sections where we introduce the Out-of-time Ordered Correlator (OTOC) as a measure for information scrambling and discuss about other related information theoretic measures as well. In this part, we also introduce the Bose Hubbard Hamiltonian and its interesting non-equilibrium properties. Then, we briefly talk about the honeycomb lattice and its linear dispersion relation.
2. The second part consists of the subsequent four sections, taking ideas from decoherence theory, we discuss how the OTOC can be described as a convolution of the Gaussian and the exponential function. Then we present results for OTOCs of our model of interest and introduce the idea of looking at the Bose-Hubbard model as an open quantum system.
3. The third part consists of the next two sections where we explore the thermodynamics of information scrambling. We connect from scrambling, work distribution and

quantum coherence.

4. In the final part, we conclude and present ideas for future work.

## 1.2 OTOCs as indicators of scrambling

One of the widely used quantities to probe scrambling is Out of Time Ordered Correlators (OTOCs). Consider a system described by a Hamiltonian  $H$  and an initial state  $|\psi\rangle$ . Given two operators  $W$  and  $V$ , the OTOC is given by

$$\langle \psi | W^+(t) V^+ W(t) V | \psi \rangle \quad (1.1)$$

where  $O(t) = e^{iHt} O e^{-iHt}$  is time evolved operator in Heisenberg picture. This is related to the commutator between  $W$  and  $V$  as

$$\langle [W(t), V]^2 \rangle = 2(1 - \text{Re}[\langle W^+(t) V^+ W(t) V \rangle]) \quad (1.2)$$

Sometimes, eq(1.2) is used as the definition of OTOC. If eq(1.1) shows a decay, then using eq(1.2), we would observe growth of the OTOC.

Consider a spin chain where  $W$  and  $V$  are operators at different sites in the chain. Initially at  $t=0$ , both the operators commute with each other. At later times, the time evolved operator starts getting contributions from operators at other sites in the chain and after a time proportional to the spatial separation of two sites,  $W(t)$  and  $V$  do not commute with each other. The operator  $W$  can be thought of as a perturbation which is evolved forward and backward in time and idea is to see what happens when you apply  $V$  before and after this perturbation. This idea is presented in figure 1.1 below. In this context of spin chains, imagine that we take two initial orthogonal states and look at the expectation value of some local operator, it can distinguish between the two states. For chaotic systems, after the thermalization time, the expectation value becomes the same for the operator in both the states. It is said that information is scrambled or lost in a manner that it cannot be recovered using local measurements on the system. In such a case, information is found

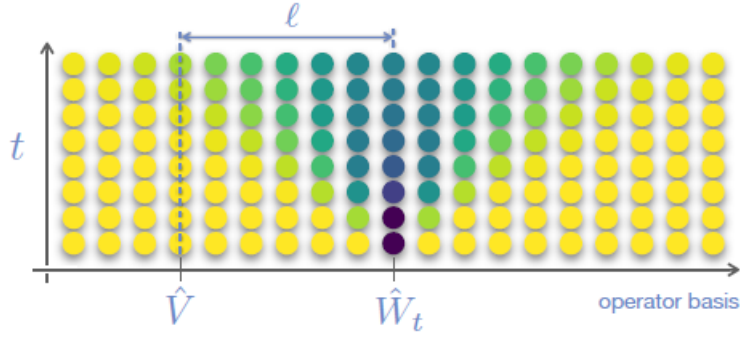


Figure 1.1: Understanding OTOC from an operator growth perspective

to spread ballistically. The speed of this ballistic information propagation is called butterfly velocity  $v_B$  and can be measured using OTOCs which behave as  $e^{\lambda_L(t-x/v_B)}$  where  $\lambda_L$  is called the Lyapunov exponent (usually for systems with finite temperature). There exists a universal bound for the Lyapunov exponent of the form  $\lambda_L \leq 2\pi k_B T/\hbar$ . Very interestingly, it was shown that black holes saturate this bound in the context of AdS/CFT.

While the OTOC is a state dependent quantity, one can also talk about state independent operator norms of commutators. The Lieb-Robinson bound provides an upper bound to the size of commutators of local operators. For the operators  $W(r,t)$  and  $V(r',0)$ ,

$$\| [W(r,t), V(r')] \| \leq C \|W\| \|V\| e^{\lambda(t - \frac{|r-r'|}{v_{LR}})} \quad (1.3)$$

where  $v_{LR}$  is known as the Lieb-Robinson velocity and acts as speed of light in these many body systems. This can be derived just based on the fact that Hamiltonian of the system is local and does not take into account the detailed nature of the interactions present in the Hamiltonian. Notice that if  $|r-r'| \ll v_{LR}t$ , then the commutator is vanishingly small. It has also been shown that the butterfly velocity (extracted from OTOCs)  $v_B$  is a state dependent Lieb-Robinson velocity [21]. For general quantum system with short range interactions that thermalize, correlations can only spread within this light cone given by the Lieb-Robinson bound. There are however, systems where this bound is rather loose and information either propagates slower or shows some sort of periodic revivals. For example, it is known that localization is possible for many-body systems in the presence of a disorder: this is known as Many-Body Localization (MBL). In this case, one finds a logarithmic light cone instead using OTOCs [10]. Another example in which information spreads differently from the ones



Figure 1.2: Illustration of Scrambling for various types of thermalisations [32]

mentioned above is quantum many-body scarred systems: here one finds a linear light cone but with periodic revivals inside light cone whenever the the initial state belongs to the subspace of scarred states [32]. These various classes are shown in Fig 1.2

Another tool that is used as a diagnostic for quantum chaotic systems is the Loschmidt Echo (LE) which is given by

$$M(t) = |\langle \psi | e^{iH_0 t} e^{i(H_0+V)t} | \psi \rangle|^2 \quad (1.4)$$

This can be understood as starting with an initial state  $|\psi\rangle$ , evolving it with the Hamiltonian of the system  $H_0$  and then evolving the same initial state with some added perturbation  $V$  and finally looking at the overlap between the two time evolved states. The idea behind studying this quantity is that small perturbations may result in drastic changes in the dynamics of the system, reminiscent of the butterfly effect. For systems with the general Hamiltonian structure  $H = H_A + H_B + \delta \sum_k V_A^k \otimes V_B^k$ , it was shown that the Haar-averaged OTOC can be written in the form of a Loschmidt Echo [28]. More precisely,

$$\overline{F_\beta(t)} = \int dA dB F_\beta(t) = \frac{1}{N^2} \sum_{\alpha, \alpha'=1} \left| \frac{1}{d_B} \text{Tr} \{ e^{i(H_B+V_\alpha)t} e^{-i(H_B+V_{\alpha'})t} \} \right|^2 \quad (1.5)$$

where  $V_\alpha = \delta \sum_k \pm V_B^k$  is a linear combination of the bath interaction operators and

$$F_\beta(t) = \langle A^\dagger(t) B^\dagger A(t) B \rangle_\beta \quad (1.6)$$

As we will eventually see, through the course of this thesis, that this way of looking at OTOCs will help us understand the nature of information scrambling in two dimensional quantum systems.

### 1.3 Other measures of information scrambling

In this section, we will look at various measures of scrambling other than OTOCs and how they are related to OTOCs.

1. Mutual Information Consider a system  $\mathcal{S}$  which is divided into two partitions A and B. The mutual information of such a setup is given by

$$I(A : B) = S_A + S_B - S_{AB} \quad (1.7)$$

where  $S_{A/B}$  is the Von-Neumann entropy of the reduced subsystems (A/B). In [26], the Haar-averaged bipartite OTOC was shown to be upper bounded by the mutual information over bi partitions.

$$1 - \overline{F_\beta(t)} \leq I(A : B)(t) \quad (1.8)$$

Since, in the context of information scrambling,  $1 - \overline{F_\beta(t)}$  is a monotonically increasing function of time, Eq(1.8) is a rigorous relationship which tells us mutual information also grows in time. This has thermodynamics implications and will be discussed in a little detail in one of the later sections

2. Tripartite Mutual Information Let A,B,C be three subregions of the lattice. Then the TMI is defined as:

$$I_3(A : B : C) = I_2(A : B) + I_2(A : C) - I_2(A : BC) \quad (1.9)$$

TMI is negative when  $I_2(A : B) + I_2(A : C) \leq I_2(A : BC)$ . In other words, information about A in BC combined is greater than sum of information about A in B and C separately. In the context of many-body systems, we start with a reference state (say a qubit) and a many body system (say a finite spin chain). Initially, the reference qubit is entangled with one of the sites in the lattice. The system then evolves unitarily and with the help of TMI, we observe how information is scrambled across the many body system. It characterizes the delocalization of quantum information. In [11], they discuss the behaviour of TMI for variety of systems such as non-integrable spin chains, MBL systems, SYK model. Their work shows that quantum information scrambling is a different idea than that of conventional quantum chaos.



These information theoretic measures have the advantage that they are independent of the choice of operators unlike the OTOC, where a Haar-average is necessary to make operator independent statements. In general, it's not very trivial to compute. In the rest of the thesis, we use these measures to quantify scrambling.

## 1.4 Bose Hubbard Model and Honeycomb Lattice

In this thesis, we study information scrambling using the Bose-Hubbard model. The Hamiltonian is given by:

$$H = -J \sum_{\langle i,j \rangle} (a_i^\dagger a_j + a_j^\dagger a_i) + \frac{U}{2} \sum_i n_i(n_i - 1) \quad (1.10)$$

where  $J$  is the nearest neighbour hopping coefficient,  $U$  is the on-site potential,  $a_i(a_i^\dagger)$  is the annihilation (creation) operator at site  $i$  in the lattice and  $n_i = a_i^\dagger a_i$  is the number of bosons at site  $i$  in the lattice. Here  $\langle i, j \rangle$  means the sum runs over nearest neighbours only.

The Bose-Hubbard model shows a second order quantum phase transition for a critical value of  $U/J$ . when  $U \ll J$  the hopping term dominates and this is called the superfluid phase. The bosons can hop around easily and form a Bose-Einstein condensate. For  $U \gg J$ , the potential term dominates, the bosons have to pay a large cost to condense into a single site and thus they tend to be localized at their respective sites in the lattice. This phase is known as the Mott-insulator phase. The Bose-Hubbard model is known to be quantum chaotic at large values of  $U/J$  or towards the right side of the critical point into the Mott phase [22]. The Bose-Hubbard model has a well-defined classical limit for fixed number of sites  $L$  and increasing particle number  $N$ . In this limit, it is equivalent to the Discrete Non linear Schrodinger equation (DNLS).

It has been shown [19] that the measures for classical chaos and measures for quantum chaos in general agree with each other. Figure 1.4, where in each heatmap, a measure of chaoticity is plotted against interaction parameter (proportional to  $U$ ) and relative energy. In the grayscale heatmap, intensity is proportional to the chaoticity- the lighter the region, the more chaotic it is. In [19], it was shown that despite being a non-integrable model,  $L=3$  and to some extent  $L=4$ , is not a strongly chaotic model but rather mixed chaos (this

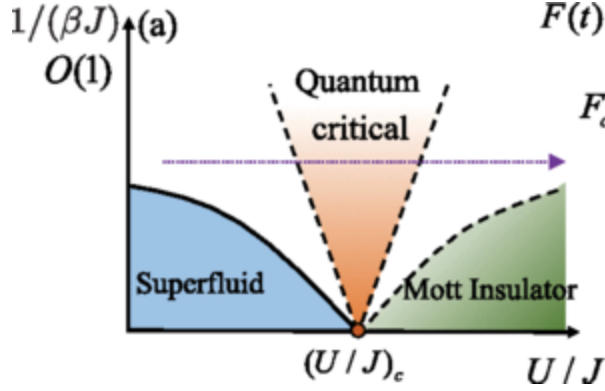


Figure 1.3: Phase diagram of Bose Hubbard model [22]

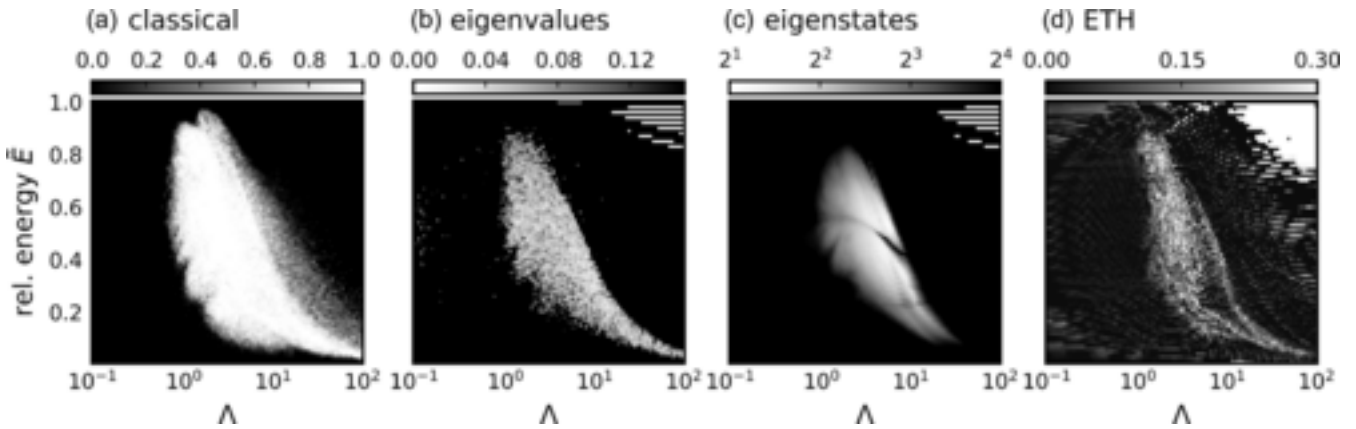


Figure 1.4: Classical and Quantum chaos indicator for the Bose Hubbard model [19]

will not be discussed in detail). The important point is that in our study, we consider the Bose-Hubbard model, with large enough sites so that it is strongly chaotic.

In [22], a modified form of OTOC for the Bose Hubbard model is computed. It is believed that a (2+1) dimensional BH model at quantum critical regime is dual to a four dimensional gravity model in anti-de Sitter space. In accordance, [22] conjectures that the Lyapunov exponent extracted from the exponential decay of the OTOC at finite temperature attains a maximum around the quantum critical region. However, the authors only show this for a one-dimensional model. In our study, we present one of the first studies of OTOC in the BHM for two dimensional geometries and explore their interesting behaviours.

The BHM is in general a very interesting model because of its non-equilibrium properties. Because it is non-integrable and its hilbert space grows exponentially with system size, it becomes increasingly difficult to perform numerical simulations using exact diagonalization

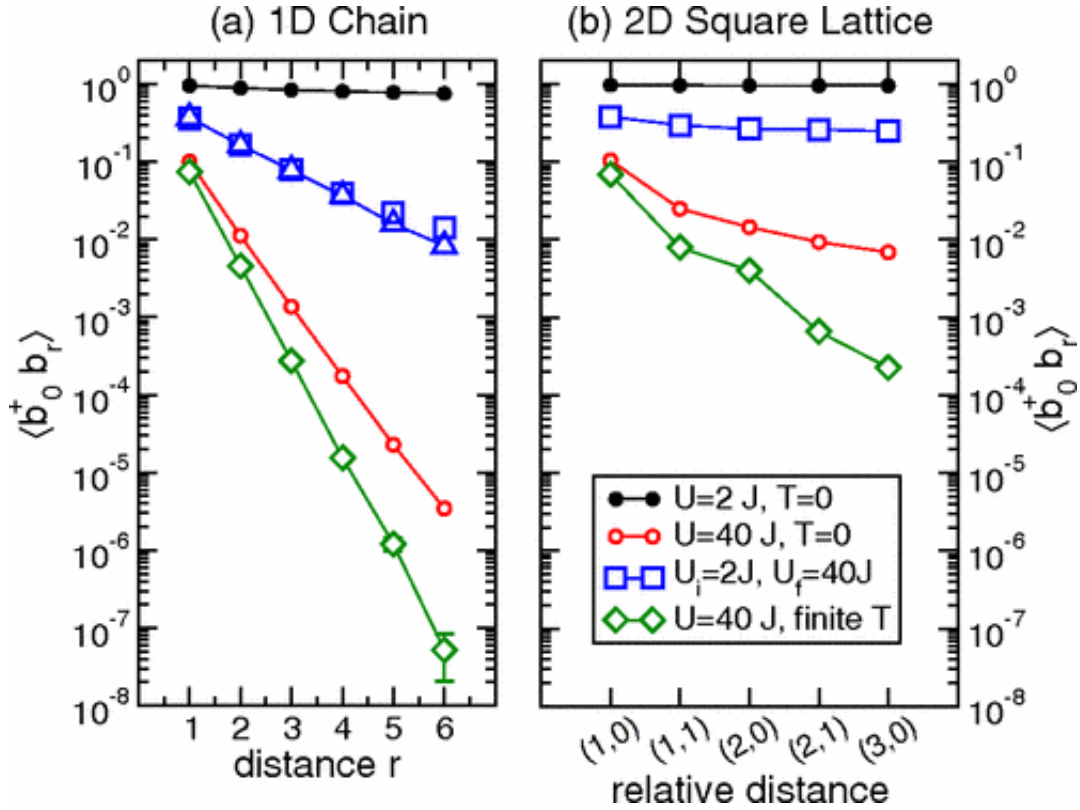


Figure 1.5: Decay of correlations with distance when  $U = 40J$  [14]

techniques and performing complicated techniques like DMRG and tensor networks are out of scope of this thesis; might be explored in a later work.

In a very interesting paper [14], the authors quenched the BHM from a superfluid to Mott insulator. They explore whether, under such a quench, the two point correlations bear memory of the initial conditions or are independent of them. They find that in spite of the non-integrability of the model, when the final quench value of  $U$  is much larger than the hopping coefficient  $J$ , the decay of correlations with distance is slower than the corresponding thermal correlations and even slower than the correlations in the ground state in the final point. In contrast to this behaviour, when final value of  $U$  is comparable to the superfluid transition ( $U \leq 6J$ ), the correlations match with that of the corresponding thermal correlations and decay faster than the ground state correlations.

These results from the paper are shown here in fig 1.5 and fig 1.6. If one neglects the quasi-particles interaction in the BHM, then the Hamiltonian can be diagonalised using a

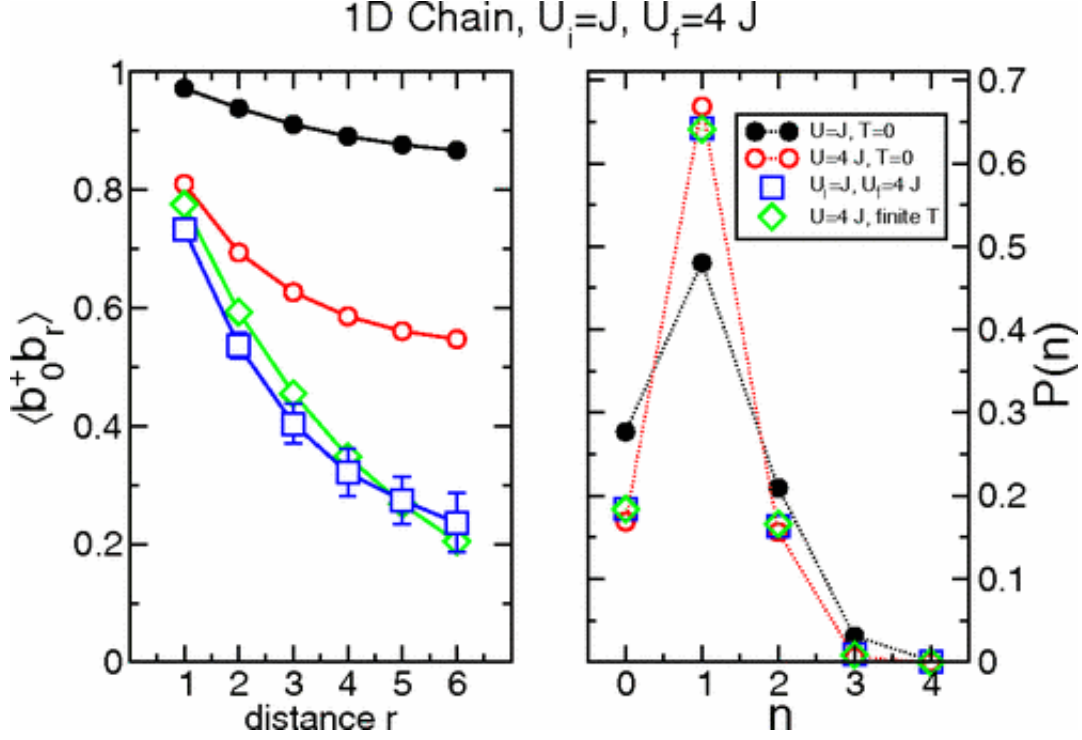


Figure 1.6: Decay of correlations with distance when  $U = 4J$  [14]

Bogoliubov transformation so that  $H = \sum_{\mathbf{k}, \alpha} \omega_{\mathbf{k}} \beta_{\alpha, \mathbf{k}}^{\dagger} \beta_{\alpha, \mathbf{k}}$  where  $\beta_{\alpha, \mathbf{k}}^{\dagger}$  is the creation operator for quasi-particle of the Mott insulator. Now, thermalization occurs due to the presence of quartic process. But since this term is a number conserving quantity, such a process is possible only when the energy is conserved. Deep into the Mott insulator regime, the energy gap  $\Delta$  is greater than half the quasi-particle bandwidth which then implies that the effects of thermalization due to the quartic process is negligible when  $U \gg J$ . Whereas, near the critical point when  $U \leq J$ , the quartic interaction has prominent contribution which leads to thermalization. This is what we see in the plots above. In one of the appendices, we show how to diagonalize the Bose Hubbard model on a hyper-cubic lattice under weak coupling.

In our study, we consider the BHM on a honeycomb lattice. Below, we discuss some interesting properties due to the lattice geometry. For simplicity, let us consider a tight-binding model of electrons with just nearest neighbour hopping terms for graphene whose Hamiltonian is given by:

$$H = -t \sum_{\langle ij \rangle} (a_i^{\dagger} b_j b_j^{\dagger} a_i) \quad (1.11)$$

where  $i(j)$  refers to sites in the sublattice A(B) in the graphene lattice and  $a, b$  are fermionic

annihilation operators. This can be rewritten as:

$$H = -t \sum_{i \in A} \sum_{\delta} (a_i^\dagger b_{i+\delta} + b_{i+\delta}^\dagger a_i) \quad (1.12)$$

where  $\delta$  is the position vector for nearest neighbours and hence in this case, the summation runs over  $\delta_1, \delta_2, \delta_3$ . Using a Fourier transformation, we can rewrite the operators in position space as

$$a_i^\dagger = \frac{1}{\sqrt{N/2}} \sum_p e^{ip \cdot r_i} a_k^\dagger \quad (1.13)$$

Substituting this into Eq [1.12](#) and after some algebraic manipulations, we obtain the following form of the Hamiltonian

$$H = \sum_{\mathbf{p}} \Psi^\dagger h(\mathbf{p}) \Psi \quad (1.14)$$

where  $\Psi^\dagger = (a_{\mathbf{p}}^\dagger, b_{\mathbf{p}}^\dagger)$  and

$$h(\mathbf{p}) = -t \begin{pmatrix} 0 & \Delta_{\mathbf{p}} \\ \Delta_{\mathbf{p}}^* & 0 \end{pmatrix} \quad (1.15)$$

is the matrix representation of the Hamiltonian and  $\Delta_p = \sum_{\delta} e^{ip \cdot \delta}$ . The energy of such a system is given by the eigenvalues of Eq [1.15](#)

$$E_{\pm}(\mathbf{p}) = \pm t \sqrt{1 + 4 \cos\left(\frac{3}{2} p_x a\right) \cos\left(\frac{3}{2} p_y a\right) + 4 \cos^2\left(\frac{\sqrt{3}}{2} p_y a\right)} \quad (1.16)$$

Eq [1.16](#) tells us that there are two energy bands given by  $E_+$  and  $E_-$ . These are plotted in Fig [1.7](#). Unlike the band gap for a square lattice, these bands are not gapped and touch each other at certain  $\mathbf{P}$  points in the momentum space; the points are known as Dirac points.

In this  $\mathbf{p}$  space, we look at the behavior of dispersion relation near the Dirac points. Consider the relative momentum  $\mathbf{k} = \mathbf{p} - \mathbf{P}$  where  $\mathbf{P}$  refers to the Dirac point. About  $\mathbf{P}$ , the Hamiltonian is then given by :

$$h(\mathbf{P} + \mathbf{k}) = v_F \begin{pmatrix} 0 & k_x + ik_y \\ k_x - ik_y & 0 \end{pmatrix} \quad (1.17)$$

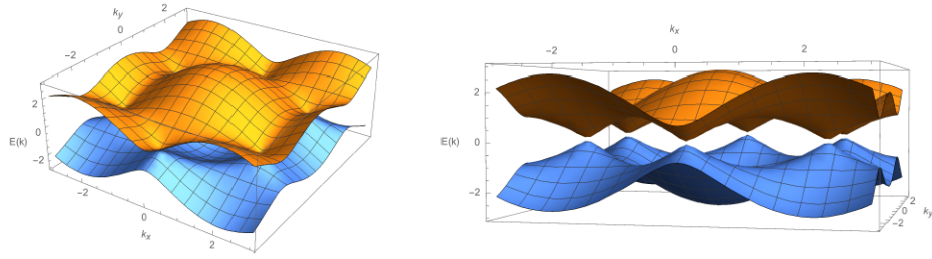


**Figure 2:** Energy bands for graphene from nearest-neighbor interactions. The bands meet at the Dirac points, at which the energy is zero.

Figure 1.7: Energy band gaps for graphene

where  $v_F \propto 3t/2$ . In terms of Pauli matrices, we can rewrite it as:

$$h(\mathbf{P}+\mathbf{k}) = v_F(k_x\sigma_x - qk_y\sigma_y) \tag{1.18}$$

This is nothing but the 2D massless Dirac Hamiltonian which describes free relativistic fermions and here the effective speed of light is given by  $v_F = \frac{3at}{2}$ . Then, it can be easily shown that the energy bands are given by:

$$E_{\pm}(\mathbf{p}) \propto |\mathbf{p}| \tag{1.19}$$

In summary, in this chapter, we have explored interesting properties of the Bose Hubbard model and the Honeycomb lattice separately. In our study, we study information scrambling dynamics of the Bose Hubbard model on a honeycomb lattice using OTOCs.

# Chapter 2

## Scrambling, Decoherence and Results

### 2.1 OTOC as a convolution function

In this section, we discuss how the decoherence function in an open system can be described using a convolution of Gaussian and exponential function and how the same function can be used to describe OTOCs as well [29]. When an isolated quantum system  $\mathcal{S}$  is kept in contact with an environment  $\mathcal{E}$ , quantum information from  $\mathcal{S}$  flows into  $\mathcal{E}$  which causes decoherence. Usually, decoherence is presumed to decay exponentially, this is not always the case. Now, consider a single spin interacting with a general environment and the Hamiltonian for the  $\mathcal{SE}$  is given by:

$$H = \lambda \sigma_z \otimes H_I + H_{\mathcal{E}} \quad (2.1)$$

where  $\sigma_z$  is the Pauli operator and the  $H_{I,\mathcal{E}}$  acts on  $\mathcal{E}$ . We assume that the composite system starts out in a product state

$$\rho_{\mathcal{SE}}(0) = \rho_{\mathcal{S}} \otimes \rho_{\mathcal{E}} \quad (2.2)$$

Let's suppose the spin system starts in an initial state  $|\psi_{\mathcal{S}}(0)\rangle = a|0\rangle + b|1\rangle$  and  $\rho_{\mathcal{E}}$  starts in an energy eigenstate  $|n\rangle$ . The decoherence factor in such a setup is given by  $r(t) = \rho_{12}(t)/(ab^*)$ . This can be rewritten in the following manner:

$$r(t) = \langle n | e^{iH_{\mathcal{E}}t} e^{(-iH_{\mathcal{E}}t + \lambda H_{\mathcal{I}\mathcal{P}})} | n \rangle \quad (2.3)$$

where  $H_{\mathcal{P}}$  is an effective perturbation proportional to  $H_I$ . Let the eigenstates of the perturbed Hamiltonian  $H_{\mathcal{E}} + \lambda H_{\mathcal{P}}$  be  $E^k$  with eigenstates given by  $|k\rangle = \sum_n C_n^k |n\rangle$ . In this case, the decoherence factor becomes :

$$r(t) = e^{iE_n t} \sum_k e^{-iE_k t} |C_n^k|^2 = e^{iE_n t} \int dE e^{-iEt} F(E, E_n) \eta(E) \quad (2.4)$$

where  $F(E, E_n) = \overline{|C_n^k|^2}$  is essentially the overlap between the perturbed and unperturbed energy eigenstates averaged over the perturbed states and  $\eta(E)$  is the global spectral density function. For Hamiltonian with few body interactions, spectral densities are given by Gaussian distributions. It was also shown that the overlap  $F(E, E_n)$  can be approximated as Lorentzian distribution and hence the decoherence factor, upto an overall oscillation can be written as a Fourier transform of the product of the Lorentzian overlap and the Gaussian spectral density.

$$r(t) \propto e^{-\tau t/2} * e^{-\sigma^2 t^2/2} \propto \sum_{\pm} e^{\pm \tau t/2} \text{Erfc}\left(\frac{\tau/2 \pm \sigma^2 t}{\sqrt{2}\sigma}\right) \quad (2.5)$$

where  $*$  denotes convolution,  $\sigma$  is the bandwidth (standard deviation) of the spectral density distribution,  $\tau$  is the width of the overlap function and Erfc is the error function. When  $\tau \gg \sigma$ , the expression reduces to exponential decay and when  $\tau < \sigma$ , the above expression reduces to a Gaussian decay. Although derived in the context of system which is described by Eq (2.1), it was shown in [29] that this description of the decoherence function is applicable to other non-trivial systems as well.

As mentioned before, in [28], it was shown that the Haar-averaged OTOC can be written as a Loschmidt Echo (Eq 1.5). Note that in the above derivation of the decoherence factor as a convolution function, the most important step is to be able to write the decoherence factor as an imperfect echo loop or in a form similar to Loschmidt Echo which is also possible for OTOCs. Hence, it is natural to think that the OTOC is also in general described by a convolution function given by:

$$\text{OTOC} = A e^{\frac{-\tau t}{2}} \text{Erfc}\left(\frac{\tau/2 - \sigma^2 t}{\sqrt{2}\sigma}\right) + B e^{\frac{\tau t}{2}} \text{Erfc}\left(\frac{\tau/2 + \sigma^2 t}{\sqrt{2}\sigma}\right) \quad (2.6)$$

where A,B are some constants which have been introduced by hand. In the next section, we will see that Eq 2.6 is indeed a suitable description for scrambling dynamics of the Bose



Hubbard lattice.

## 2.2 Results

We use Krylov subspace methods to compute OTOCs for this model. In one of the appendices, we mention the theory of these methods used in numerics.

In Fig 2.1 and Fig 2.2, we show the OTOC for the one dimensional Bose-Hubbard with  $L=6$  sites and  $N=6$  bosons with periodic boundary conditions in two different phases characterised by the value  $U/J$ . The geometry is same as one hexagon. As the OTOC, in general, is a complex quantity, here we choose to plot the absolute value of the OTOC. Note that, even if we choose to plot only the real part, the behavior will be the same with some slight change in the visible magnitude, because in all the data obtained, the imaginary part is negligible. The sites chosen for the operators are any two nearest neighbours. Since, it's a 1D ring with 6 sites, any pair of nearest neighbours would have the same OTOC.

We observe that for  $U \ll J$  (Fig 2.1), the OTOC shows large recurrences and there is no exponential or fast decay, which is the characteristic for chaotic systems or systems with fast scrambling. On the other hand, for  $U \gg J$  (Fig 2.2), the OTOC decays rapidly and oscillates about some small mean value. As, we will see, these oscillations are due to the small size of the 1 hex lattice. The contrasting rapid decay of the OTOC implies that information scrambles very fast as the system enters into the Mott insulator phase and becomes chaotic as compared to its behaviour in the Superfluid phase where it does not show any chaotic behaviour where  $U \ll J$ . Hence, we find that Out-of-Time Ordered Correlators are able to distinguish between the two phases of the Bose-Hubbard model. However, it is not possible to characterize both the phases with the help of OTOC since quantities like Lyapunov exponent and Butterfly velocity (which we will compute for  $U \gg J$ ) are clearly not defined for the Superfluid phase.

In Fig 2.3,  $|\text{OTOC}|$  for various values of  $U/J$  are shown. We find that starting from the superfluid phase, as we keep on increasing  $U/J$ , the system goes more to the right side of the quantum critical point and it starts decaying faster.

Next, we plot the change in mutual information for the Bose-Hubbard as a function of

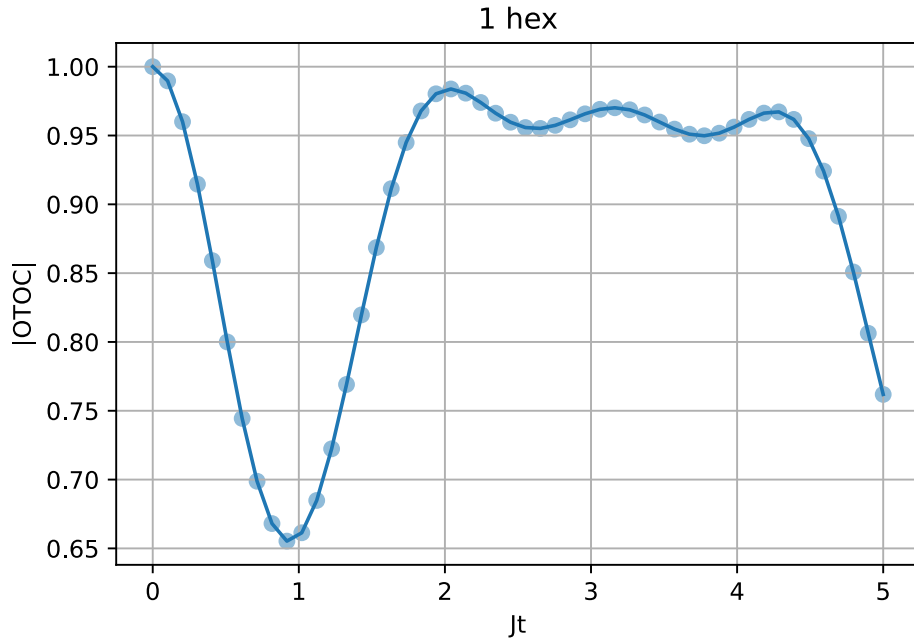


Figure 2.1:  $|\langle a_1(t)^\dagger a_2^\dagger a_1(t) a_2 \rangle_\psi|$  for the one dimensional Bose Hubbard model with  $N=6$ ,  $L=6$  for  $U/J=0.25$ ,  $|\psi\rangle = |1, 1, 1, 1, 1, 1\rangle$

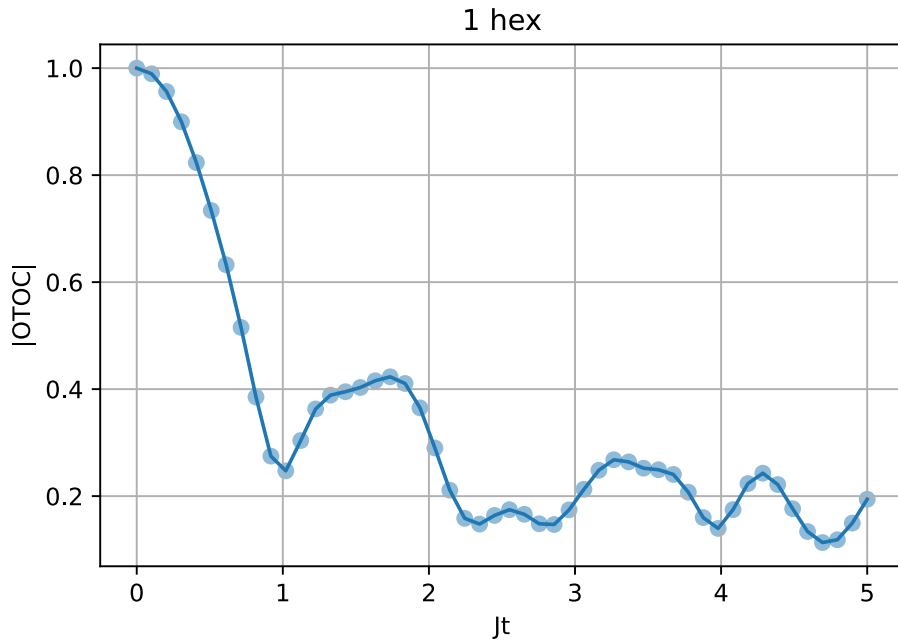


Figure 2.2:  $|\langle a_1(t)^\dagger a_2^\dagger a_1(t) a_2 \rangle_\psi|$  for the one dimensional Bose Hubbard model with  $N=6$ ,  $L=6$  for  $U/J=4$ ,  $|\psi\rangle = |1, 1, 1, 1, 1, 1\rangle$

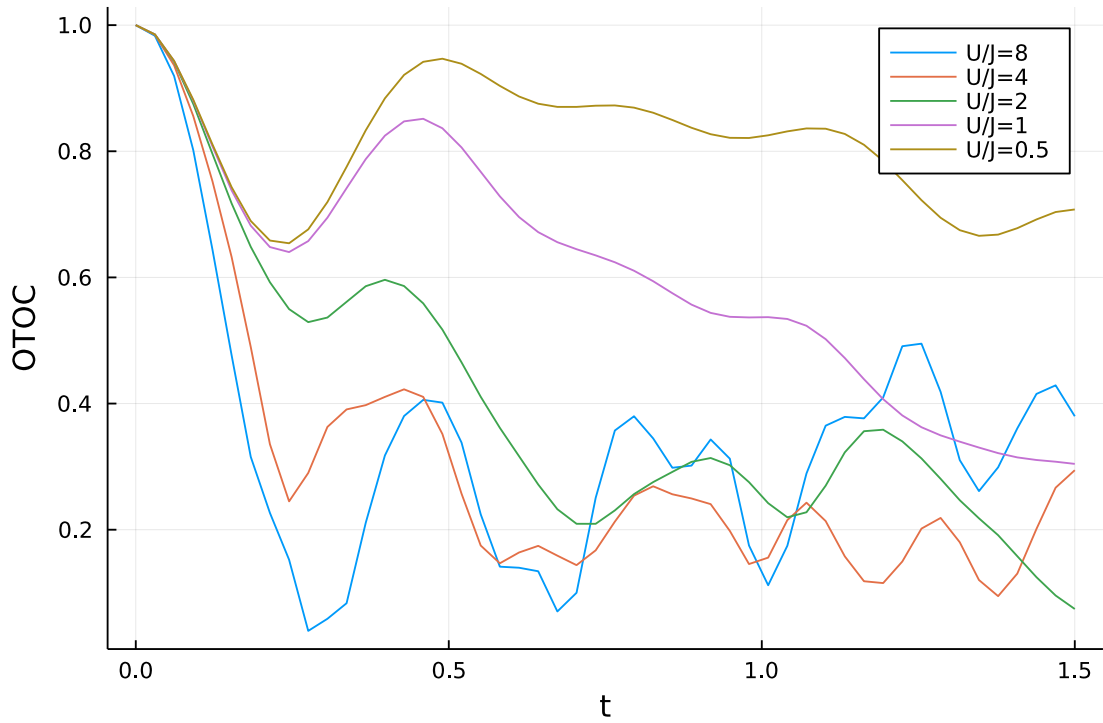


Figure 2.3:  $|\langle a_1(t)^\dagger a_2^\dagger a_1(t) a_2 \rangle|$  for the one dimensional Bose Hubbard model with  $N=6$ ,  $L=6$  for a range of coupling strengths

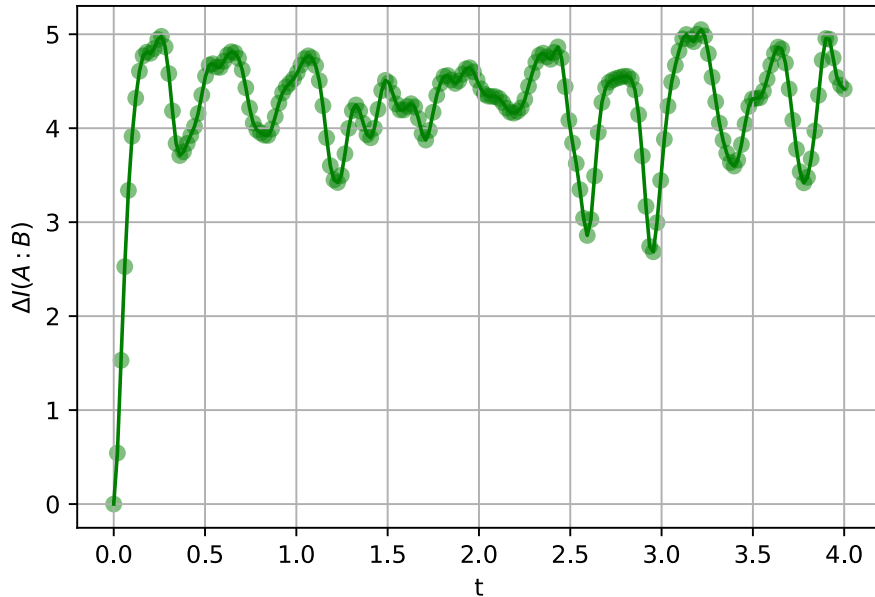


Figure 2.4: Change in mutual information for the one dimensional Bose Hubbard model with  $N=6$ ,  $L=6$   $\Delta I(A : B)$  over equal partitions A and B for  $U/J=4$

time in Fig 2.4, which as mentioned before is also an indicator of information scrambling. We divide the 1 hex lattice into equal partition with subsystem A containing the first 3 sites and subsystem B containing the rest of the 3 sites. Starting with the initial state  $|\psi\rangle = |1, 1, 1, 1, 1, 1\rangle$ , we compute  $\Delta I(A : B) = I(A : B)(t) - I(A : B)(0) = I(A : B)(t)$ . We observe a rapid initial growth followed by oscillations about some mean value.

To verify Eq 1.8, we plot the change in  $1 - \text{Re}\{OTOC\}$  and  $\Delta I(A : B)$  at early times in Fig 2.5. It is interesting to see that the inequality in Eq 1.8 is obeyed even without taking the Haar-average. This tells us that there is a high probability that OTOC formed from any two randomly chosen operators shows behavior similar to the Haar averaged OTOC. Thus, it saves us from the trouble of explicitly computing the Haar measure for our system in order to observe scrambling behavior. It was shown in [1] that a related version of the OTOC, when Haar averaged, probes the ground state entanglement and hence should be able to detect quantum phase transitions. We find clear evidence for this statement as mentioned above.

Next, we compute the Tripartite Mutual Information (TMI) for the Bose Hubbard model.

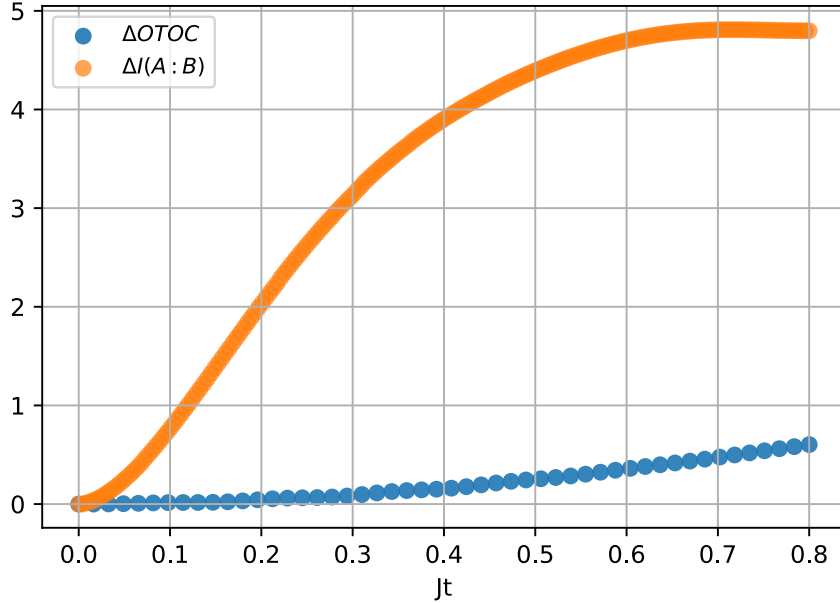


Figure 2.5: Comparison between change in OTOC and change in Mutual Information for the one dimensional Bose Hubbard model with  $N=6$ ,  $L=6$

In this setup, we take a reference boson and entangle it with one of the bosons in the lattice. The bosons in the lattice evolve via the usual Bose Hubbard Hamiltonian. Subsystem A consists of just the single reference boson whose initial state does not change with time. The 6 site lattice, which is the one hexagon setup here, is divided into three subsystems: B containing the one site which is entangled with subsystem A, C containing the next 2 sites, D containing the last 3 sites. The initial state considered here is :  $|\psi\rangle = (|0\rangle_A \otimes |1\rangle_B + |1\rangle_A \otimes |0\rangle_B) |1, 1, 1, 1, 1\rangle_{CD}$ . The expression for TMI is given by :  $I_3(A : B : C) = S_A + S_B + S_C - (S_{AB} + S_{AC} + S_{BC}) + (S_{ABC} = S_D)$  since we the initial state  $|\psi\rangle$  is a pure state. Note that one cannot take only two partitions of the lattice which evolves via Bose Hubbard Hamiltonian because that would lead to  $I_3(A : B : C) = 0$  as the terms cancel because of symmetry of the Von-Neumann entropy. The behaviour of TMI is shown in Fig [2.6](#).

In summary, we have verified signatures of quantum information scrambling using OTOCs, Bi-partite Mutual information and Tripartite Mutual information in the Bose-Hubbard model when the system is on the right hand side of the quantum critical point towards the Mott Insulator phase.

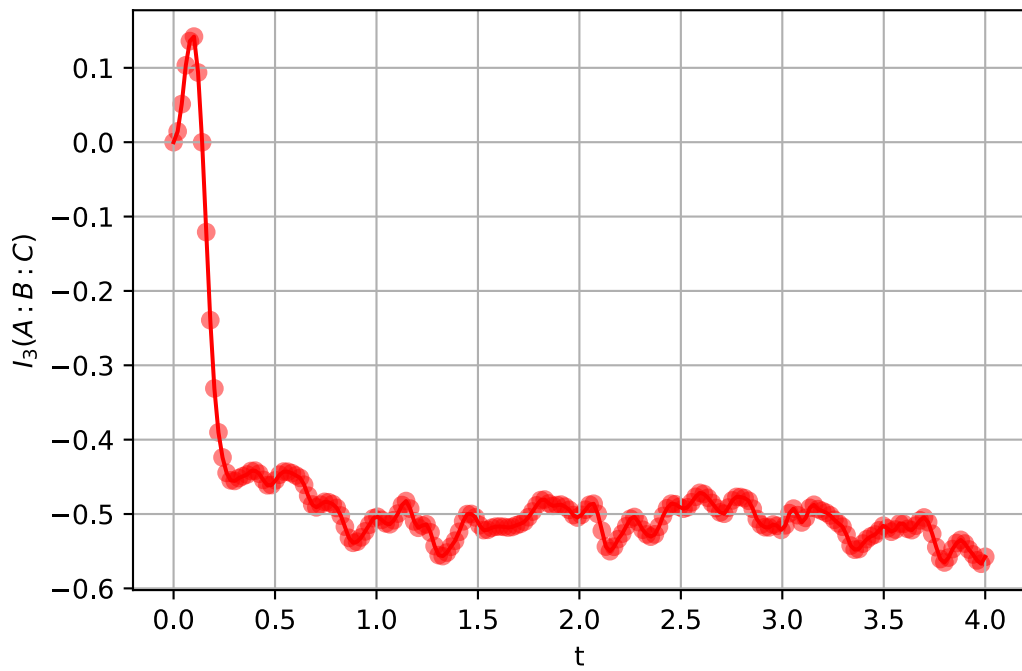


Figure 2.6: Tripartite Mutual Information  $I_3(A : B : C)$  for the one dimensional Bose Hubbard model with  $N=6$ ,  $L=6$  where  $A$  is a reference boson and  $B,C$  are partitions of the 6 site lattice

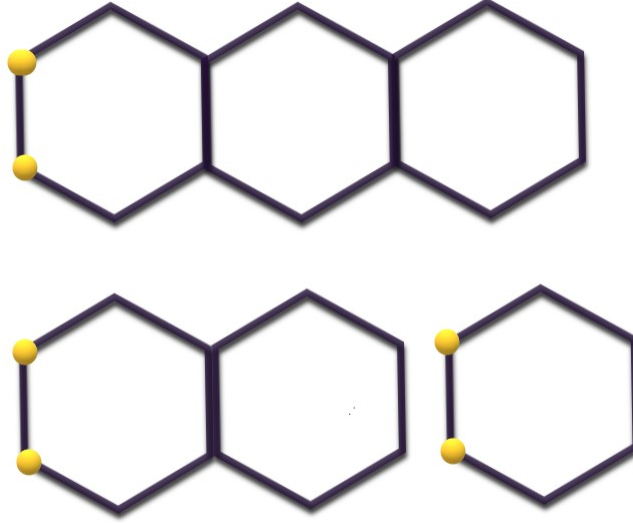


Figure 2.7: Configuration of two dimensional hex lattices for case 1 where OTOCs for all hex lattices match

Now, we increase the size of the hexagonal lattices and compute OTOCs for two dimensional lattices with two hexagons and three hexagons respectively. We also consider two possible geometrical arrangement of the three hexagonal lattice. In the following three different cases are mentioned which reveal interesting behavior of the OTOCs.

### 2.2.1 All OTOCs agree

In Fig 2.7 above, we show three different configurations for the hex lattices with the yellow dots representing the two sites over which local operators are defined for the OTOCs. Fig 2.8 shows plots for the OTOC for the 1 hex, 2 hex and 3 hex lattices. The initial state considered here is  $|\psi\rangle = |1, 1, 1, 1, 1, 1\rangle$  The OTOC is in general a complex number, here we show the modulus of the OTOC.

We find that for all the three lattices, the initial decay of the OTOC is exactly the same but they differ in their long time behavior. We also see that the oscillations, which followed after the rapid decay, in the case of 1 hex lattice is due to its small size since OTOCs for 2 hex and 3 hex do not show any such oscillations and just decay to zero.

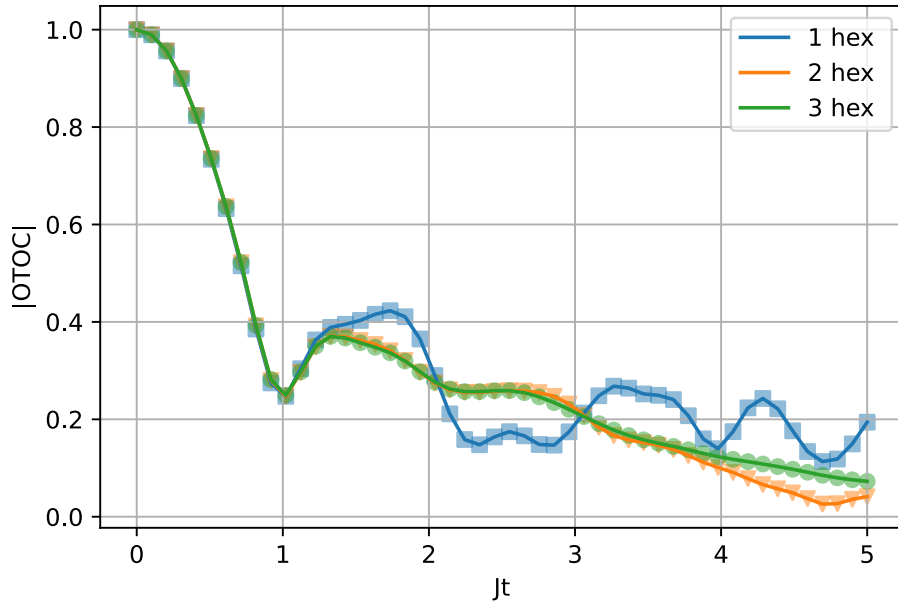


Figure 2.8: Behavior of OTOCs for the case ( Fig (2.7) ) when all OTOCs agree for the initial state  $|\psi\rangle = |1, 1, 1, 1, 1\rangle$

## 2.2.2 Strip Configuration

In Fig 2.9, we show the strip configuration for the three lattices. It is named so, because to increase the size of the lattice, hexagons are stacked right next to each other in a horizontal fashion. Fig 2.10 shows the plot of OTOCs vs time for the initial state  $|\psi\rangle = |1, 1, 1, 1, 1, 1\rangle$ .

We find that in this arrangement, the neighbourhood around the sites considered is different in contrast to the previous case where the neighbourhood was same for all three lattices. The OTOCs clearly differ from each other for different lattices. The data fits for these are shown in Fig 2.11, 2.12, 2.13. For the case of 1 hex and 2 hex, the OTOC shows a clear Gaussian decay. For 3 hex, it fits best to both the convolution function and Gaussian decay but at the same time it's very close to the exponential decay.

Later, using the fitting parameters obtained, we show that one gets a negative scrambling velocity for the Gaussian decay and hence the convolution function is the best description for the OTOC in the 3 hex case.



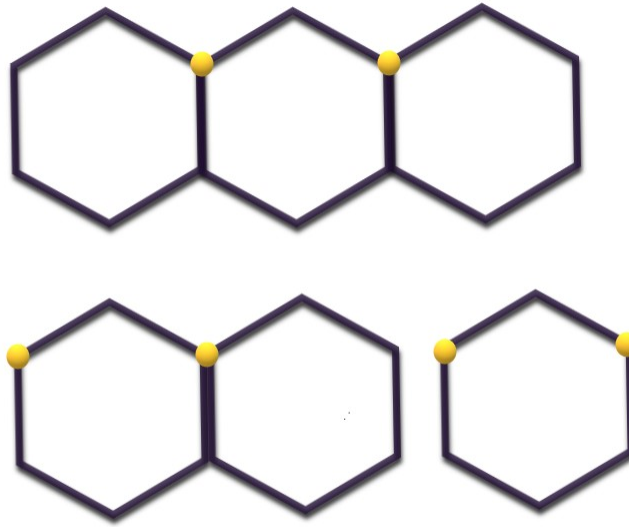


Figure 2.9: Strip Configuration for the two dimensional hex lattices

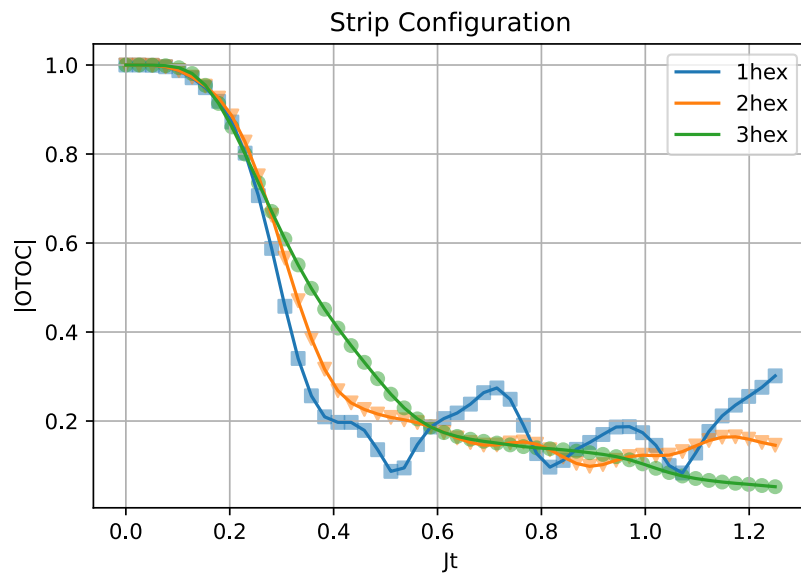


Figure 2.10: Behavior of OTOCs for the strip configuration ( Fig (2.9) ) for the initial state  $|\psi\rangle = |1, 1, 1, 1, 1\rangle$

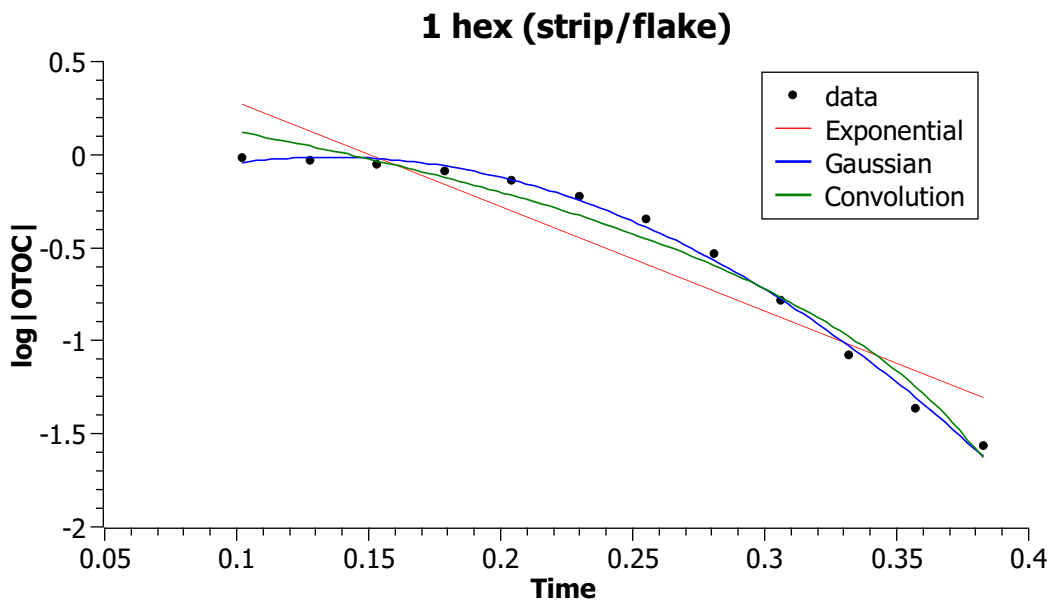


Figure 2.11: Data fit for OTOC of 1 hex strip configuration ( Fig (2.10) )

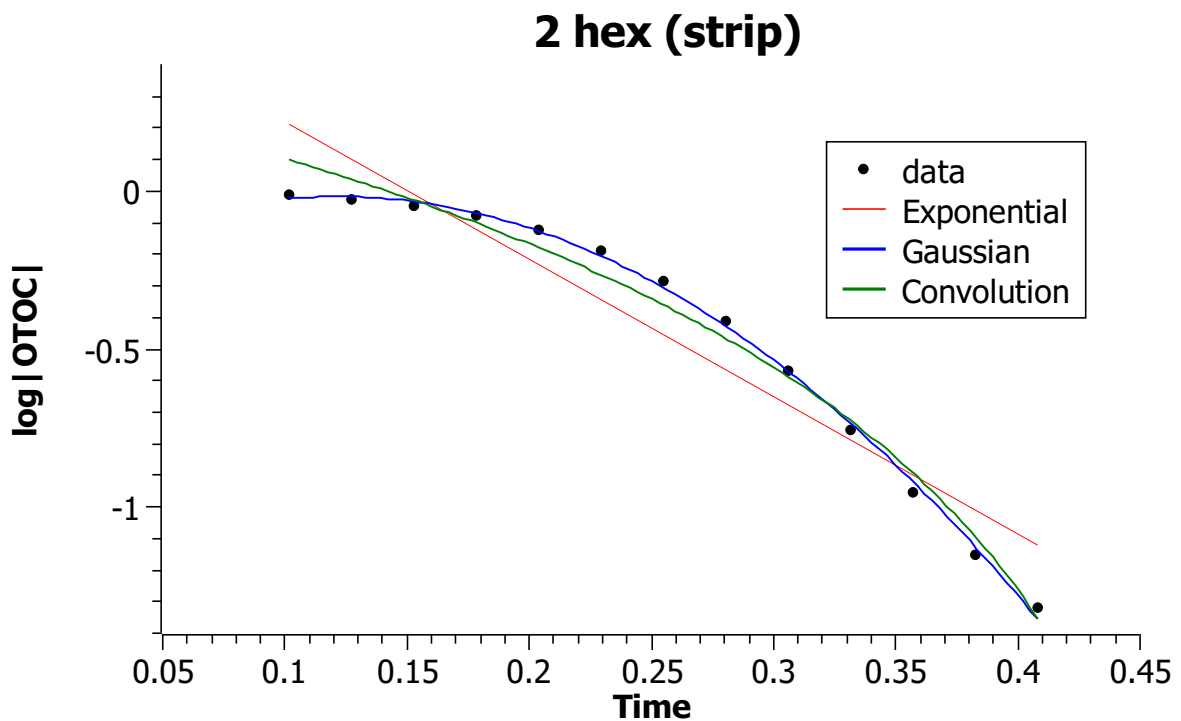


Figure 2.12: Data fit for OTOC of 2 hex strip configuration ( Fig (2.10) )

### 3 hex(Strip)

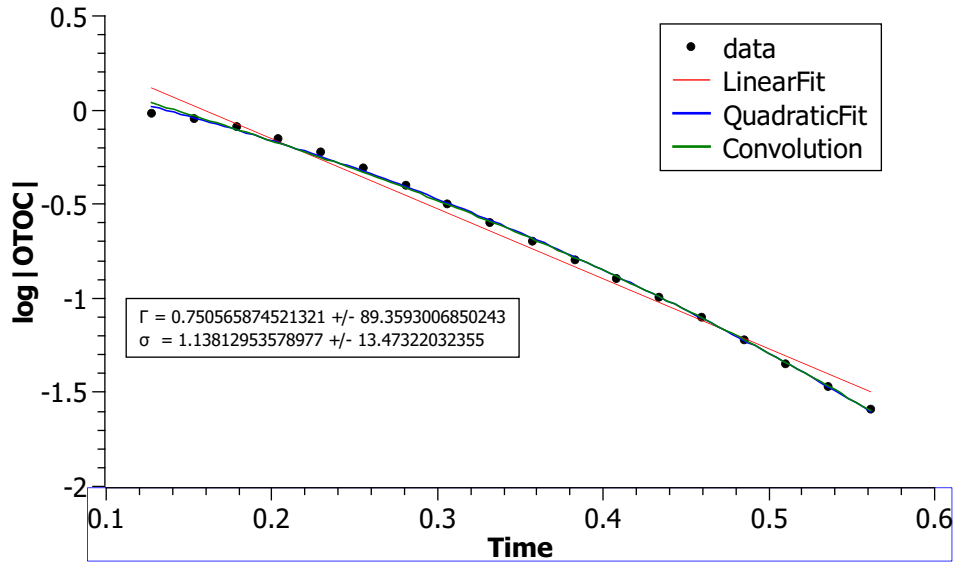


Figure 2.13: Data fit for OTOC of 3 hex strip configuration ( Fig (2.10) )

### 2.2.3 Flake Configuration

This is the second possible arrangement of three hexagons in a lattice. The configuration is shown in Fig 2.14. The OTOCs differ for different lattices and the plots for OTOCs and their data fits are shown below in Fig 2.15 and Fig 2.16, 2.17 respectively. Here, we find that the OTOC is best fit to both convolution and Gaussian decay but is very close to the exponential decay as well. The scrambling velocities obtained in both these cases is negative and hence the convolution function best describes the scrambling behavior in both 2 hex and 3 hex lattices. The 1 hex case here is the same as that of the strip configuration and hence not discussed again.

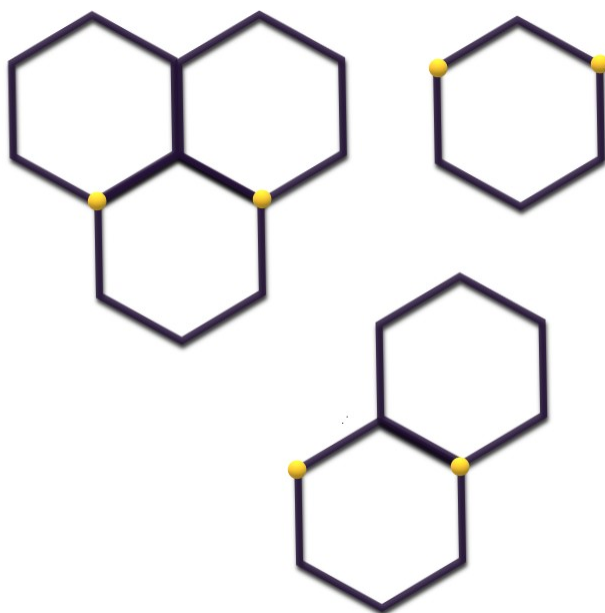


Figure 2.14: Flake configuration for two dimensional hex lattices

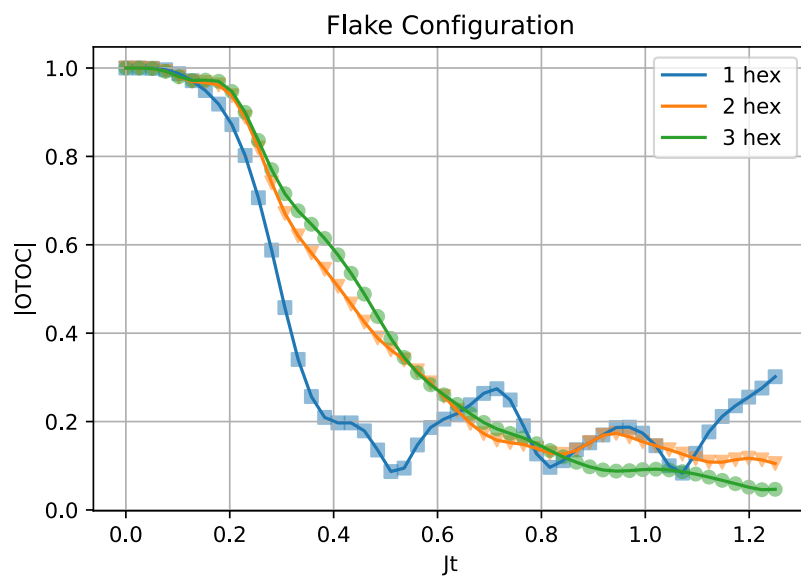


Figure 2.15: Behavior of OTOCs for the flake configuration ( Fig (2.14) ) for the initial state  $|\psi\rangle = |1, 1, 1, 1, 1\rangle$

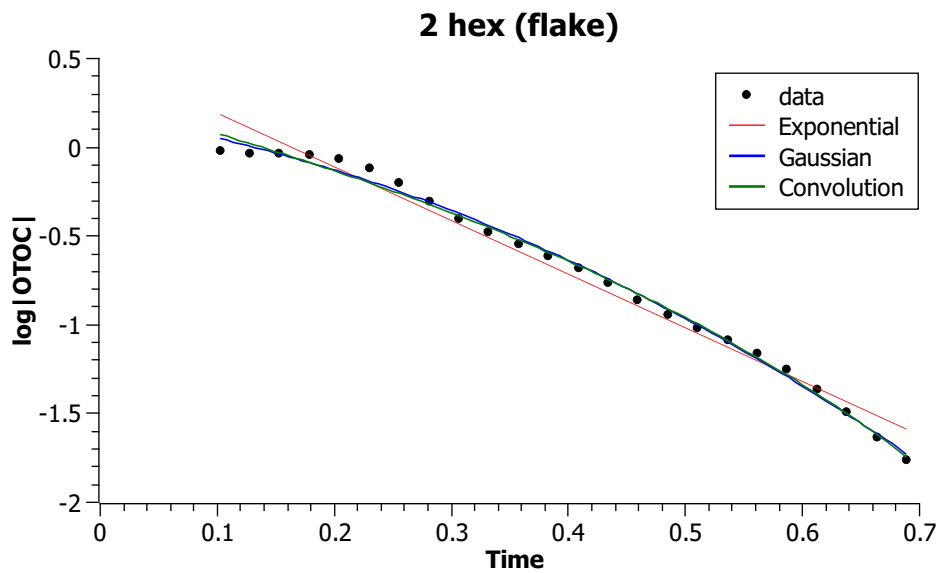


Figure 2.16: Data fit for OTOC of 2 hex flake configuration ( Fig (2.15) )

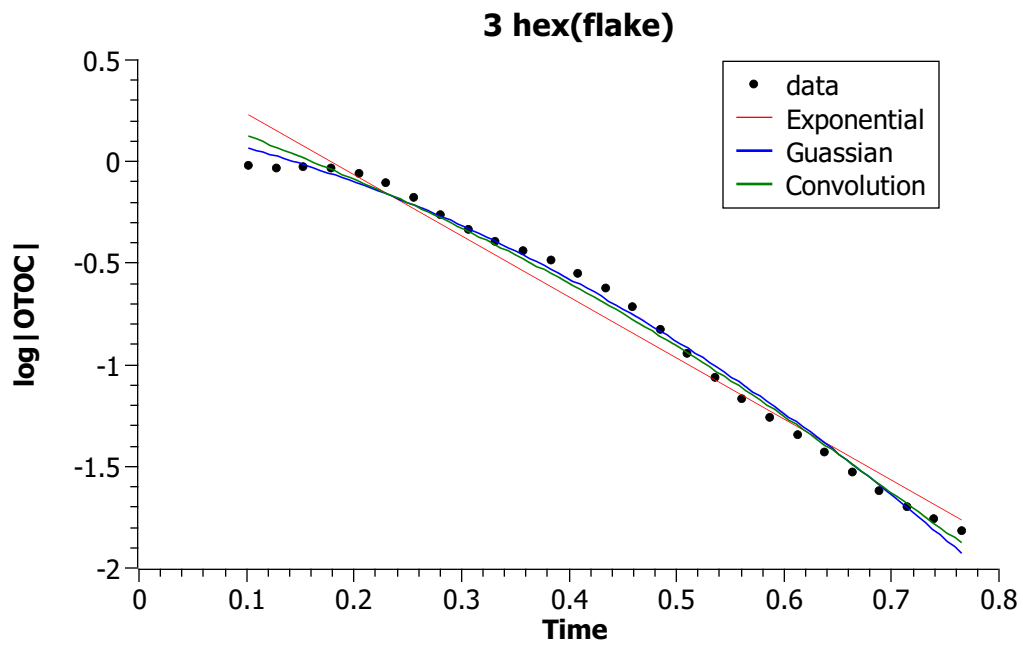


Figure 2.17: Data fit for OTOC of 3 hex flake configuration ( Fig (2.15) )

Now, we try to quantify the initial decays of the OTOCs for all three hex lattices, extract the exponent of the decay and their respective scrambling velocity.

1. **Gaussian decay:**

$$\text{OTOC} = e^{\lambda(t - \frac{|x|}{v})^2} \quad (2.7)$$

Taking log on both sides, we can write:

$$\begin{aligned} \log(\text{OTOC}) &= \lambda(t - |x|/v)^2 \\ &= \lambda t^2 - \frac{2\lambda|x|t}{v} + \frac{\lambda|x|^2}{v^2} \\ &= at^2 + bt + c \end{aligned} \quad (2.8)$$

where  $\lambda = a$  ,  $v = -\frac{2\lambda|x|}{b}$

2. **Exponential Decay:**

$$\text{OTOC} = e^{\lambda(t - \frac{|x|}{v})} \quad (2.9)$$

Taking log on both sides, we can write:

$$\begin{aligned} \log(\text{OTOC}) &= \lambda(t - \frac{|x|}{v}) \\ &= \lambda t - \frac{\lambda|x|}{v} \\ &= at + b \end{aligned} \quad (2.10)$$

where  $\lambda = a$  ,  $v = -\frac{\lambda|x|}{b}$

The exponent of decay ( $\lambda$ ) and velocity( $v$ ) extracted from the OTOCs (Which is also discussed above) are presented in the tables [2.1](#), [2.2](#) below.

Under the 'fit type' column, the text marked green refers to the function that fits best to the data. However, there are cases where Gaussian is a better fit than the exponential but the velocity extracted using Gaussian gives rise to a negative velocity (marked in red) and hence exponential becomes a better choice. As can be seen from the fit plots, these are exactly the cases where the Gaussian behavior of the OTOC starts to converge towards the exponential decay and is better described by the convolution function.

geometry	lattice	fit type	$\lambda$	$v$
a)strip	1 hex	Gaussian	-26.310	14.754
		exponential	-5.619	13.299
b)strip	2 hex	Gaussian	-16.352	16.389
		exponential	-16.351	8.194
c)strip	3 hex	Gaussian	-3.072	-9.591
		exponential	-3.734	12.551

Table 2.1: Parameters for strip configuration

geometry	lattice	fit type	$\lambda$	$v$
a)flake	2 hex	Gaussian	-2.536	-9.848
		exponential	-3.024	12.218
b)flake	3 hex	Gaussian	-2.330	-9.481
		exponential	-3.003	11.205

Table 2.2: Parameters for flake configuration

Next, we also present the data for parameters of the convolution function in Eq (2.6) in the Tables 2.3, 2.4 below.

We find that when  $\tau \ll \sigma$ , OTOC is well described using a Gaussian decay function whereas as soon as  $\tau > \sigma$ , the OTOC is better described by the convolution function and starts converging to an exponential decay which we do not observe in our 3 hex models. To see the complete transition from Gaussian to exponential, larger lattices need to be explored which are beyond the scope of Krylov subspace methods used here.

In summary, we have shown using numerical techniques that the OTOC for a Bose Hubbard model on a honeycomb lattice hints at a Gaussian to exponential decay transition which can be described using a convolution of both the decay functions. We also observe that in these two dimensional systems, the behavior of the OTOC strongly depends upon the neighbourhood of the sites chosen for local operators. Also, this way of looking at

lattice	configuration	$\tau$	$\sigma$	$\frac{\tau}{\sigma}$
a) 1 hex	strip	1.822	0.122	14.934
b) 2 hex	strip	1.707	0.163	10.472
c) 3 hex	strip	0.751	1.138	0.660

Table 2.3: Convolution parameters for strip configuration

lattice	configuration	$\tau$	$\sigma$	$\frac{\tau}{\sigma}$
a) 1 hex	flake	1.822	0.122	14.934
b) 2 hex	flake	0.495	0.875	0.566
c) 3 hex	flake	0.667	0.954	0.699

Table 2.4: Convolution parameters for flake configuration

OTOC implies that information scrambling which describes how localised information gets delocalized over the degrees of freedom of a quantum many body system can be equivalently thought of as considering one or two sites as the system, rest of the sites as the bath and decoherence between system and environment this way becomes information scrambling within the unitary quantum system. To understand this more concretely, we present a master equation considering a subsystem of the Bose Hubbard lattice as our system and rest as our bath and then try to compute the decoherence function explicitly.

## 2.3 Bose Hubbard model as an open system

Let us begin by reviewing the derivation of master equation for open quantum systems. Consider the full system + environment described by the total Hamiltonian

$$H = H_S + H_B + H_I \quad (2.11)$$

where  $H_S$  and  $H_B$  describe the free Hamiltonian of the system and bath respectively.  $H_I$  is the Hamiltonian describing the interaction between system and bath. After applying the usual Born-Markov approximations, we arrive at the following Markovian quantum master equation:

$$\frac{d}{dt}\rho_S(t) = - \int_{-\infty}^{\infty} ds \text{tr}_B[H_I(t), [H_I(t-s), \rho_S(t) \otimes \rho_B]] \quad (2.12)$$

Next, we decompose the interaction Hamiltonian as follows:

$$H_I = \sum_{\alpha} A_{\alpha} \otimes B_{\alpha} \quad (2.13)$$

Assuming that  $H_S$  has a discrete spectrum, we define the projection operator projecting into



the eigenvalue  $\epsilon$  as  $\Pi(\epsilon)$ . Then, we can also define

$$A_\alpha(\omega) = \sum_{\epsilon' - \epsilon = \omega} \Pi(\epsilon) A_\alpha \Pi(\epsilon') \quad (2.14)$$

The sum in the above expression is over all possible energy eigenvalues  $\epsilon'$  and  $\epsilon$ . Using the above definition, it is straightforward to show

$$[H_S, A_\alpha(\omega)] = -\omega A_\alpha(\omega) \quad (2.15)$$

As a consequence, the operators in the interaction picture becomes:

$$e^{iH_S t} A_\alpha(\omega) e^{-iH_S t} = e^{-i\omega t} A_\alpha(\omega) \quad (2.16)$$

Hence, the interaction picture interaction Hamiltonian can be written as:

$$H_I(t) = \sum_{\alpha, \omega} e^{-i\omega t} A_\alpha(\omega) \otimes B_\alpha(t) \quad (2.17)$$

where  $B_\alpha(t) = e^{iH_B t} B_\alpha e^{-iH_B t}$ . Now substituting Eq (2.17) into Eq (2.12), we get

$$\frac{d}{dt} \rho_S(t) = \sum_{\omega, \omega'} \sum_{\alpha, \beta} e^{i(\omega' - \omega)t} \Gamma_{\alpha\beta}(\omega) (A_\beta(\omega) \rho_S(t) A_\alpha^\dagger(\omega') - A_\alpha^\dagger(\omega') A_\beta(\omega) \rho_S(t)) + h.c \quad (2.18)$$

where

$$\Gamma_{\alpha\beta}(\omega) = \int_0^\infty ds e^{i\omega s} \langle B_\alpha^\dagger(t) B_\beta(t-s) \rangle \quad (2.19)$$

Additionally, if we assume that  $[H_B, \rho_B] = 0$ , then we find that the bath correlation functions become homogeneous in time

$$\langle B_\alpha^\dagger B_\beta(t-s) \rangle = \langle B_\alpha^\dagger(s) B_\beta(0) \rangle \quad (2.20)$$

Now, we perform the secular approximation or the rotating wave approximation where we

neglect all the terms where  $\omega' \neq \omega$  and only keep terms with  $\omega' = \omega$ . Then we have

$$\frac{d}{dt}\rho_S(t) = \sum_{\omega} \sum_{\alpha,\beta} \Gamma_{\alpha\beta}(\omega)(A_{\beta}(\omega)\rho_S(t)A_{\alpha}^{\dagger}(\omega) - A_{\alpha}^{\dagger}(\omega)A_{\beta}(\omega)\rho_S(t)) + h.c \quad (2.21)$$

In literature, the Fourier transform of bath correlation functions into real and imaginary parts as follows:

$$\Gamma_{\alpha\beta}(\omega) = \frac{1}{2}\gamma_{\alpha\beta}(\omega) + iS_{\alpha\beta}(\omega) \quad (2.22)$$

$$\gamma_{\alpha\beta}(\omega) = \Gamma_{\alpha\beta}(\omega) - \Gamma_{\beta\alpha}^*(\omega) = \int_{-\infty}^{\infty} ds e^{i\omega s} \langle B_{\alpha}^{\dagger}(s)B_{\beta}(0) \rangle \quad (2.23)$$

With all of the above definitions, we can finally write the following master equation

$$\frac{d}{dt}\rho_S(t) = -i[H_{LS}, \rho_S(t)] + \mathcal{D}(\rho_S(t)) \quad (2.24)$$

where we have defined the Lamb shift Hamiltonian as

$$H_{LS} = \sum_{\omega} \sum_{\alpha\beta} S_{\alpha\beta}(\omega)A_{\alpha}^{\dagger}(\omega)A_{\beta}(\omega) \quad (2.25)$$

and the Dissipator is defined as:

$$\mathcal{D}(\rho_S) = \sum_{\omega} \sum_{\alpha\beta} \gamma_{\alpha\beta}(\omega)(A_{\beta}(\omega)\rho_S A_{\alpha}^{\dagger}(\omega) - \frac{1}{2}\{A_{\alpha}^{\dagger}(\omega)A_{\beta}(\omega), \rho_S\}) \quad (2.26)$$

With all the tools required at hand, we now try to rewrite the Bose Hubbard Hamiltonian in Eq(1.10) in the form of Eq(2.11). Denote the site in the lattice which we consider as system by  $S$ . Then the system Hamiltonian is given by:

$$H_S = \frac{U}{2}n_S(n_S - 1) \quad (2.27)$$

The Hamiltonian for the bath is

$$H_B = -J \sum_{\langle i \neq S, j \rangle} (a_i^{\dagger}a_j + a_j^{\dagger}a_i) + \frac{U}{2} \sum_{i \neq S} n_i(n_i - 1) \quad (2.28)$$

And the interaction Hamiltonian between the system and bath is :

$$H_I = -J \sum_{S,j} (a_S^\dagger a_j + a_j^\dagger a_S) \quad (2.29)$$

To understand this better, let's consider the situation where  $S$  has three nearest neighbours on the lattice :  $S + 1, S + 2, S + 3$ . Then explicitly writing the interaction Hamiltonian

$$H_I = -J(a_S^\dagger \otimes (a_{S+1} + a_{S+2} + a_{S+3}) + a_S \otimes (a_{S+1}^\dagger + a_{S+2}^\dagger + a_{S+3}^\dagger)) \quad (2.30)$$

$$= -J(a_S^\dagger \otimes B_{S,1} + a_S \otimes B_{S,2}) \quad (2.31)$$

where  $B_{S,1} = a_{S+1} + a_{S+2} + a_{S+3}$  and  $B_{S,2} = a_{S+1}^\dagger + a_{S+2}^\dagger + a_{S+3}^\dagger = B_{S,1}^\dagger$ . These will be the bath operators which will contribute to the bath correlation functions defined in Eq(2.23). The Lindblad operators can be chosen to be  $a_S$  and  $a_S^\dagger$ .

But for the Bose Hubbard Hamiltonian, some assumptions are not satisfied which are needed to write a Lindblad master equation (2.24). These are listed below

1. Secular Approximation The Lindblad operators  $a_S$  and  $a_S^\dagger$  do not satisfy Eq(2.15) and as a consequence Eq(2.16) does not hold either. Note that because of Eq(2.16), we were able to get  $e^{i(\omega' - \omega)t}$  in Eq (2.18) which then allowed us to perform the secular approximation. Without it, it is not at all trivial to carry out this approximation. It is also important to note that it is because of the quartic term in the potential that we are not able to satisfy (2.15), (2.16); had it been a simple harmonic oscillator, this would not have been the case and we would be able to write the master equation in Lindblad form.
2. Further Consequences One of the good things about Lindblad master equation is that starting from an equation involving integrating elements of density matrix, we finally have an equation that just involves integrating just a correlation function. This is because usually Eq(2.15) is satisfied; that allows us to bring the dependence of the time variable  $s$  out of the system's operator expressions and transfer it to the bath operators which are then traced over and become a number. The fact that Eq(2.15) does not get satisfied means none of this can be done and the time dependence of  $s$  stays within.
3. Time Dependence If secular approximation is performed, then it removes the time

dependence  $t$  from the RHS of the differential equation except for the system's time dependent density matrix for which we are solving.

4. Born-Markov approximation This will never be satisfied for the finite size systems. The important part is that the time scales of what we define as system and bath might not be well separated to perform the Markov approximation. But to perform numerical simulation, we might have to do it anyway and hope that it does not affect our predictions.

Nevertheless, none of this prevents us from writing a Master equation considering one or few of the sites in the lattice as our system and rest as bath and also compute the bath correlation functions.

For this purpose, we do not project the interaction picture operators onto the system's eigenenergies, that is we don't do Eq (2.14). The only reason such a projection was used is because if we find suitably projected operators which obey the commutation relation (2.15), it helps for the cases mentioned above. In their absence, we can write the following master equation

$$\frac{d}{dt}\rho_S(t) = \int_0^\infty ds \sum_{\alpha,\beta} \Gamma_{\alpha\beta}(t,s) (A_\beta(t-s)\rho_S(t)A_\alpha^\dagger(t) - A_\alpha^\dagger(t)A_\beta(t-s)\rho_S(t)) + h.c \quad (2.32)$$

where

$$\Gamma_{\alpha\beta}(t,s) = \langle B_\alpha^\dagger(t)B_\beta(t-s) \rangle \quad (2.33)$$

where to be more precise about the conditions satisfied by Bose Hubbard, we should have replaced the upper limit of the integral from  $\infty$  to  $t$ . But that might make the computation of the differential equation even harder. We use Eq (2.32) to numerically solve the differential equation and integrate over all time dependent elements of the density matrix to get the RHS.

Next, we divide the whole lattice into system, containing the same two sites as in the OTOCs, and bath with the rest of the sites. If we go by the dynamics of Bose Hubbard, the number of bosons in both the sites of the system can be anything from 0 to  $N$  where  $N$  is the number of bosons in the full  $\mathcal{SE}$ . This is because even if the bath has no bosons left,

the system can decay due to quantum fluctuations of the bath. The only issue is that if the number of bosons in the bath  $N_B$  vary immensely at different times, the bath operators in the correlation function (2.33) will evolve using different Hamiltonians in the sense that the sizes of the Hamiltonian matrix used in the numerics will be different at different times and hence need to be kept tracked of. What we can do instead is we keep the  $N_b$  same at all times and we allow for some minimal excitations within the system. We essentially set the rule, that if  $N_a$  number of bosons leak into the system from the bath, we do not consider any change in the dynamics of the bath when it comes to computing (2.33) and we evolve it with the number of bosons it had to begin with. Consequently, we only allow  $N_a$  number of bosons to be distributed between the two sites. For example, if  $N_a = 2$ , then the possible states for  $\mathcal{S}$  are  $\{|1, 0\rangle, |0, 1\rangle, |1, 1\rangle, |2, 0\rangle, |0, 2\rangle\}$ . That way even if we are integrating all elements of the density matrix with time to solve Eq (2.32), we would only have to do it for small size matrices.

In the study of OTOCs, we find that for the 2 hex case, the OTOCs differ for the strip and flake configurations. While in the case of a strip, the OTOC is better described by a Gaussian decay, for the case of a flake, the OTOC starts to converge towards the exponential decay and is better described by the convolution function. It would be great if we find the same behavior for decoherence function of the two configurations as well. This would essentially mean that because of the orientation of interaction sites for particular sites in the lattice, we get different behaviors of the decoherence function and hence would also explain the dynamics of the OTOCs as well.

Note that we would need to compute the bath correlation functions numerically for our effective open system. For the 2 hex lattice configurations, we remove the nodes for system sites from the hexagonal graph and compute two point correlation function corresponding to bath operators from the interaction Hamiltonian on this modified. The results are shown in Fig (2.18) and Fig (2.18) below. The plots are labelled by the jump process, whose parameters are specific system operators, associated with the corresponding bath correlation functions. While these by themselves do not help us with the physics of the problem at hand, we need them to solve the master equation (2.32). The exact numerical solution is left for future work.

2 hex strip bath correlation functions

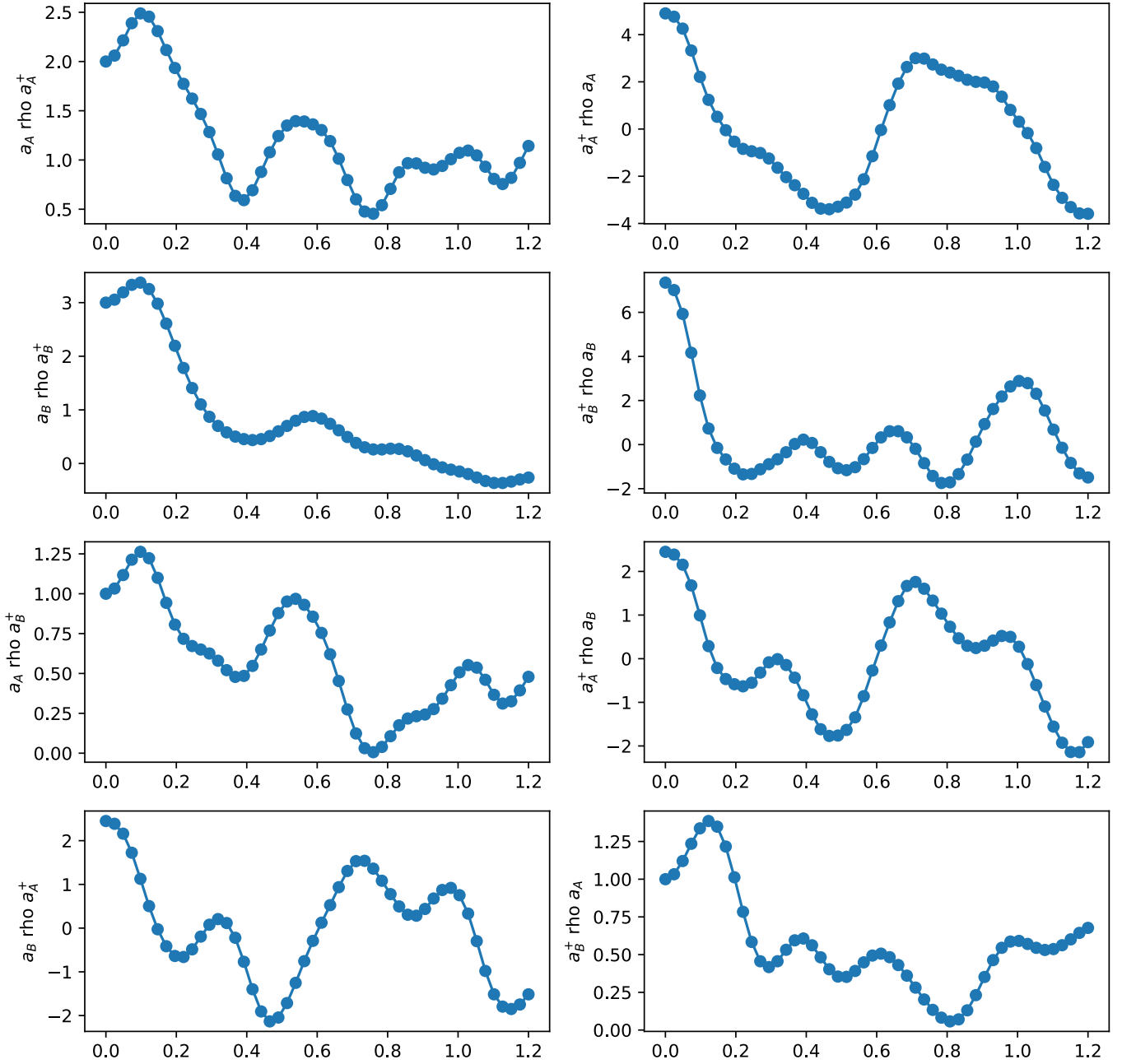


Figure 2.18: Bath correlation functions for strip configuration

2 hex flake bath correlation functions

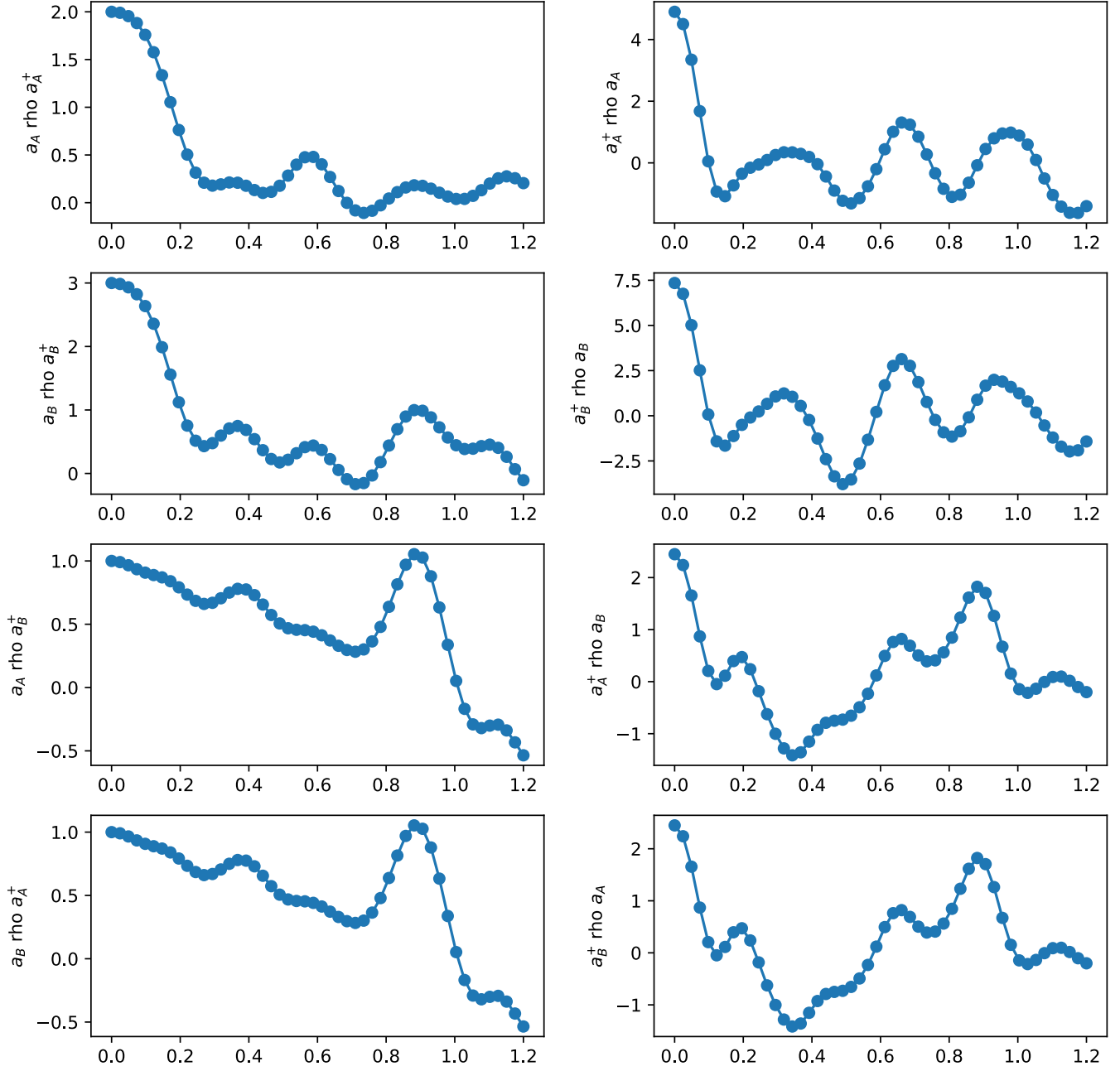


Figure 2.19: Bath correlation functions for flake configuration





# Chapter 3

## Thermodynamics of Scrambling and Concluding Remarks

### 3.1 Work distribution, Coherence and Scrambling

In this section, we briefly describe quantum work and the entropy of quantum work. Further, we also mention a few attempts made as a part of the thesis to relate information scrambling, OTOCs and work done in quantum systems ; hence try to make some progress towards the thermodynamic interpretation of quantum information scrambling.

In quantum mechanics, work is defined using the two point measurement approach. This is described as follows. Consider a quantum system initially described by the density matrix  $\rho$ . At the beginning of the protocol, the Hamiltonian is given by  $H(0) = \sum_n E_n^0 |n_0\rangle \langle n_0|$ . The system is then evolved using the work protocol using the unitary  $U$  such that at the end of the process, the state of the system evolves to  $\rho(t) = U\rho U^\dagger$  and the final Hamiltonian is given by  $H(t) = \sum_m E_m^t |m_t\rangle \langle m_t|$ . In such a scenario, the two point measurement involves making two projective measurements at beginning and end of the work protocol. The difference between the initial and final measurements is defined as work done during the process. Clearly, the work defined this way is described using a probability distribution given as

follows:

$$P(W) = \sum_{n,m} p_n p_{m_t|n_0} \delta_{W, E_m^t - E_n^0} \quad (3.1)$$

where  $p_n = \langle n_0 | \rho | n_i \rangle$  is the probability of getting  $|n_0\rangle$  in the first measurement and  $p_{n|m} = |\langle m_t | U | n_0 \rangle|^2$  is the probability of getting  $|m_f\rangle$  in the second measurement given that one has already got  $|n_i\rangle$  in the first measurement i.e the transition probability. The work defined this way also obeys results from stochastic thermodynamics such as the Jarzynski equality which is given by

$$\langle e^{-\beta W} \rangle = e^{-\beta \Delta F} \quad (3.2)$$

where  $F$  is the free energy. Note that even if Eq (3.2) looks the same as the classical Jarzynski equality, quantum work is very different from its classical counterpart. There is no hermitian operator whose eigenvalues match with the classical values of work. The reason for this is that the Hamiltonian does not commute with itself at various times:  $[H(0), H(t)] \neq 0$ . Usually, the moments or cummulants of work are used to study work distribution in quantum systems. In a recent work [12], the authors looked at the entropy of probability distribution describing quantum work,  $H_W$  given by:

$$H_W = - \sum_W P(W) \ln P(W) \quad (3.3)$$

The authors further showed that the entropy of work distribution obeys the following bound

$$H_W \leq 2S(\bar{\rho}) + C(\bar{\rho}) \quad (3.4)$$

where  $\bar{\rho} = \sum_n \langle n_0 | \rho | n_0 \rangle |n_0\rangle \langle n_0|$  is the initial density matrix of the system dephased in the basis of initial Hamiltonian  $H(0)$  and  $S(\bar{\rho}) = -\text{tr} \bar{\rho} \ln \bar{\rho}$  is the Von-Neumann entropy . The relative entropy of coherence(REC) of a state  $\sigma$  in the basis  $|m'_t\rangle = U^\dagger |m_t\rangle$  is given by:

$$C(\sigma) = S(D_t(\sigma)) - S(\sigma) \geq 0 \quad (3.5)$$

where  $D_t(\sigma) = \langle m'_t | \sigma | m'_t \rangle |m'_t\rangle \langle m'_t|$  is the state  $\sigma$  dephased in the basis  $|m'_t\rangle$ . In what follows below, we have made an attempt to further bound the entropy of work. To do this, let us start by rewriting the  $D_t(\sigma)$  in Eq (3.4) using its definition mentioned above.

$$D_t(\bar{\rho}) = \sum_m \langle m'_t | \bar{\rho} | m'_t \rangle | m'_t \rangle \langle m'_t | \quad (3.6)$$

$$= \sum_m \langle m_t | U \bar{\rho} U^\dagger | m_t \rangle | m'_t \rangle \langle m'_t | \quad (3.7)$$

$$= \sum_m \langle m_t | \bar{\rho}(t) | m_t \rangle | m'_t \rangle \langle m'_t | \quad (3.8)$$

$$= \sum_m \bar{\rho}(t)_{m_t, m_t} | m'_t \rangle \langle m'_t | \quad (3.9)$$

where we have used the definition of  $|m'_t\rangle$  above and  $\bar{\rho}(t)_{m_t, m_t} = \langle m_t | \bar{\rho}(t) | m_t \rangle$ . Since entropy remains unchanged under a unitary transformation, we can write:

$$S(D_t(\bar{\rho})) = S\left(\sum_m \bar{\rho}(t)_{m_t, m_t} | m'_t \rangle \langle m'_t | \right) \quad (3.10)$$

$$= S\left(\sum_m \bar{\rho}(t)_{m_t, m_t} U^\dagger | m_t \rangle \langle m_t | U \right) \quad (3.11)$$

$$= S\left(\sum_m \bar{\rho}(t)_{m_t, m_t} | m_t \rangle \langle m_t | \right) \quad (3.12)$$

Keeping in mind the basis in which the Hamiltonian of the system is diagonal at different times of the work protocol, we can define:

$$\bar{\rho} = \sum_n \langle n_0 | \rho | n_0 \rangle | n_0 \rangle \langle n_0 | = \rho^{diag}(0) \quad (3.13)$$

$$\rho^{diag}(t) = \sum_m \langle m_t | \rho(t) | m_t \rangle | m_t \rangle \langle m_t | = \rho(t)_{m_t, m_t} | m_t \rangle \langle m_t | \quad (3.14)$$

Now, notice that  $\rho(t)$  contains more information than  $\bar{\rho}(t)$ . Since  $\bar{\rho}(t)$  is already dephased in the initial basis of  $H_i$ , we can write using Eq [\(3.14\)](#)

$$S(\rho^{diag}(t)) \leq S\left(\sum_m \bar{\rho}(t)_{m_t, m_t} | m_t \rangle \langle m_t | \right) = S(D_t(\bar{\rho})) \quad (3.15)$$

Finally, we can write the change in relative entropy of coherence during the work protocol as:

$$\Delta C = S(\rho^{diag}(t)) - S(\rho(t)) - (S(\rho^{diag}(0)) - S(\rho(0))) \quad (3.16)$$

$$\leq S(D_t(\bar{\rho})) - S(\rho(t)) - (S(\bar{\rho}) - S(\rho(0))) \quad (3.17)$$

$$= S(D_t(\bar{\rho})) - S(\bar{\rho}) - (S(\rho(t)) - S(\rho(0))) \quad (3.18)$$

Hence,

$$\Delta C \leq C(\bar{\rho}) - \Delta S \quad (3.19)$$

## 3.2 Mutual Information, Scrambling and Open systems

In this section, we briefly mention how bipartite mutual information can be used to describe information scrambling in open systems.

In most parts of this thesis, OTOCs have been used to study and characterize information scrambling. However, one major drawback with using these quantities is that the choice of operators in the OTOC is somewhat ambiguous and arbitrary. One has to take averages over operator space in order to make mathematically precise statements. Performing these averages can turn out to be technically difficult. Also, it might be difficult to distinguish between information scrambling and decoherence using OTOCs. Hence in [\[25\]](#), it was proposed that mutual information be used to study scrambling in open systems. Here, we briefly mention some of their results and ideas. Consider a closed quantum system  $\mathcal{S}$ , here the mutual information between two partitions of the system A and B is given by:

$$I(A : B) = S_A + S_B - S_{AB} \quad (3.20)$$

where  $S_{i \in \{A,B\}} = -\text{tr} \sum_i \rho_i \ln \rho_i$  is the Von-Neumann entropy. When the dynamics (in this context, the scrambling dynamics) is unitary, the change in mutual information is given by:

$$\Delta I = I(t) - I(0) = \Delta S_A + \Delta S_B \quad (3.21)$$

Now, we consider the setup for an open system where the system  $\mathcal{S}$  interacts with an environment  $\mathcal{E}$ . We assume that the the initial state of the composite system  $\mathcal{SE}$  is given by the product state  $\rho_0 = \rho_{\mathcal{S}}(0) \otimes \rho_{\mathcal{E}eq}$  where  $\rho_{\mathcal{E}eq} = e^{-\beta H}/Z$  is the thermal Gibbs state at inverse temperature  $\beta$ . In such a case, Eq (3.21) is not valid anymore since the dynamics of  $\mathcal{S}$  is no longer unitary and the change in mutual information becomes:

$$\Delta I = \Delta S_A + \Delta S_B - \Delta S_S \quad (3.22)$$

One of the main results from [25] is the following equation:

$$I(\mathcal{S} : \mathcal{E}) + \Delta S_{ex} + D(\rho_{\mathcal{E}} || \rho_{\mathcal{E}}^{eq}) = \Delta S_S \quad (3.23)$$

where

$$\Delta S_{ex} = \text{tr}\{(\rho_{\mathcal{E}} - \rho_{\mathcal{E}}^{eq}) \ln \rho_{\mathcal{E}}^{eq}\} = \beta \langle Q \rangle \quad (3.24)$$

Eq (3.24) is the heat exchanged between  $\mathcal{S}$  and  $\mathcal{E}$  and

$$D(\rho_{\mathcal{E}} || \rho_{\mathcal{E}}^{eq}) = \text{tr}\{\rho_{\mathcal{E}} \ln \rho_{\mathcal{E}}\} - \text{tr}\{\rho_{\mathcal{E}} \ln \rho_{\mathcal{E}}^{eq}\} \quad (3.25)$$

Eq (3.25) is the Kullback-Leibler divergence. Eq (3.23) tells us that the deviation from unitary scrambling dynamics comes from three factors: the correlations between  $\mathcal{S}$  and  $\mathcal{E}$ , heat exchanged between  $\mathcal{S}$  and  $\mathcal{E}$  and the deviation of  $\mathcal{E}$  from thermal equilibrium.

In [25], they also come up with a statement for second law of thermodynamics for scrambling. We describe it here.

Here, we perform two point projective measurements on the system and environment at time  $t = 0$  and  $t = \tau$ . Then we define the following observables.

$$\omega_{\mathcal{S}}^{\mu\nu} = \ln(p_{\mathcal{S}}^{\mu}) - \ln(p_{\mathcal{S}}^{\nu}) \quad (3.26)$$

where  $\mu$  and  $\nu$  are the outcomes of the initial and final projective measurements. Similarly, for  $\mathcal{E}$ , we define

$$\omega_{\mathcal{E}}^{mn} = \ln(p_{\mathcal{E}}^m) - \ln(p_{\mathcal{E}}^n) \quad (3.27)$$

Then the following statement holds

$$\langle \omega_S \rangle + \langle \omega_{\mathcal{E}} \rangle = \Delta I(\mathcal{S} : \mathcal{E}) + \Delta C(\mathcal{S}) \quad (3.28)$$

where  $C$  is the relative entropy of coherence as introduced in the previous section in the context of entropy of work distributions. It is interesting to see the Relative entropy of Coherence (REC) appear both in the context of information scrambling and work distribution. Eq (3.19) derived above was an attempt to connect the change in the REC to the REC of the dephased initial density matrix which sets a bound on the entropy of work. These ideas can be explored further to get a better thermodynamic understanding of information scrambling.

# Chapter 4

## Conclusion

In this thesis, we have understood the scrambling behavior in a two dimensional quantum system. We started with showing that the one dimensional Bose-Hubbard model becomes quantum chaotic as we increase the coupling strength to take the system towards the right hand side of the quantum critical point into the Mott insulator phase. This result using OTOC is verified additionally with Mutual Information and Tripartite Mutual Information.

Then, we move into two dimensional hexagonal geometries where the behavior of the OTOC is greatly influenced by the neighbourhood of the two local sites which are chosen for operators in the expression for OTOC. We consider two different configurations which we call strip and flake configurations. A Gaussian to near-exponential transition is observed as we increase the size of the lattice as well as in the case when we move from a strip to hex arrangement of the hexagons.

Using the fact that both the Haar-averaged OTOC and decoherence function can be written in the form of a Loschmidt Echo, we argue as well as verify using numerics that the OTOC from the Bose-Hubbard model on honeycomb lattices can be described using a convolution of Gaussian and exponential function and thus reduces to a Gaussian or exponential decay in certain limits of a relevant coupling strength. During the near-exponential transition, the OTOC shows the convolution behaviour. We believe that the scrambling dynamics will fully transition into exponential decays with further increase in size but this needs to be verified using more sophisticated method of numerics.

Next, we have looked at Bose Hubbard system as an open quantum system by considering few of the sites in the lattice as the system and rest of the sites as bath. It is shown that such a setup does not satisfy the conditions for it be written down as a Lindblad master equation. We then present a suitable master integral-differential master equation which can be solved to obtain the decoherence function. We built the framework for the configuration and leave the results for future work. The hope is that we recover the same Gaussian to exponential transition behavior with the decoherence function.

Then, we briefly discussed quantum work distribution and a newly introduced concept called entropy of work which is bounded by the Relative Entropy of Coherence(REC) of the system. It is shown that this REC is related to change in REC mentioned in the context of scrambling of system connected to a bath. The characteristic work function itself can be written as a Loschmidt echo function. All of these results hint towards a connection between information scrambling and work done quantum systems which needs to be explored in detail. A good starting point would be to compute work distribution for our two dimensional Bose Hubbard lattices using the numerical tools we already have. We also leave this for future work.

In summary, we have shown with concrete numerical evidence that the scrambling dynamics in the unitary Bose-Hubbard model shows features of decoherence function of an open quantum system. This is the idea that the way information scrambles or spreads from a localised site in the lattice to the rest of the lattice can be equivalently thought of as the way information decoheres from a quantum system into its connected bath. Of course, as mentioned above, this claim needs to be further verified by computing the decoherence function for the Bose-Hubbard model. We have also presented some interesting future directions of 'work' for a consistent thermodynamic interpretation of information scrambling.



# Bibliography

- [1] Namit Anand and Paolo Zanardi. “BROTOCs and Quantum Information Scrambling at Finite Temperature”. In: *Quantum* 6 (June 2022), p. 746. ISSN: 2521-327X. DOI: [10.22331/q-2022-06-27-746](https://doi.org/10.22331/q-2022-06-27-746). URL: <https://doi.org/10.22331/q-2022-06-27-746>.
- [2] Arpan Bhattacharyya, Lata Kh Joshi, and Bhuvanesh Sundar. “Quantum information scrambling: from holography to quantum simulators”. In: *The European Physical Journal C* 82.5 (2022), p. 458.
- [3] Michele Campisi and John Goold. “Thermodynamics of quantum information scrambling”. In: *Physical Review E* 95.6 (2017), p. 062127.
- [4] Anffany Chen et al. “Quantum holography in a graphene flake with an irregular boundary”. In: *Physical review letters* 121.3 (2018), p. 036403.
- [5] Mitsutoshi Fujita et al. “Towards a holographic Bose-Hubbard model”. In: *Journal of High Energy Physics* 2015.4 (2015), pp. 1–39.
- [6] Martin Gärttner et al. “Measuring out-of-time-order correlations and multiple quantum spectra in a trapped-ion quantum magnet”. In: *Nature Physics* 13.8 (2017), pp. 781–786.
- [7] Nicole Yunger Halpern. “Jarzynski-like equality for the out-of-time-ordered correlator”. In: *Physical Review A* 95.1 (2017), p. 012120.
- [8] Pavan Hosur et al. “Chaos in quantum channels”. In: *Journal of High Energy Physics* 2016.2 (2016), pp. 1–49.
- [9] Yichen Huang, Yong-Liang Zhang, and Xie Chen. “Out-of-time-ordered correlators in many-body localized systems”. In: *Annalen der Physik* 529.7 (2017), p. 1600318.

- [10] Yichen Huang, Yong-Liang Zhang, and Xie Chen. “Out-of-time-ordered correlators in many-body localized systems”. In: *Annalen der Physik* 529.7 (2017), p. 1600318. DOI: <https://doi.org/10.1002/andp.201600318>. eprint: <https://onlinelibrary.wiley.com/doi/pdf/10.1002/andp.201600318>. URL: <https://onlinelibrary.wiley.com/doi/abs/10.1002/andp.201600318>.
- [11] Eiki Iyoda and Takahiro Sagawa. “Scrambling of quantum information in quantum many-body systems”. In: *Phys. Rev. A* 97 (4 Apr. 2018), p. 042330. DOI: [10.1103/PhysRevA.97.042330](https://doi.org/10.1103/PhysRevA.97.042330). URL: <https://link.aps.org/doi/10.1103/PhysRevA.97.042330>.
- [12] Anthony Kiely et al. *Entropy of the quantum work distribution*. 2022. arXiv: [2210.07896](https://arxiv.org/abs/2210.07896) [quant-ph].
- [13] Alexei Kitaev. *A simple model of quantum holography (part 2)*. Kavli Institute for Theoretical Physics Program: Entanglement in Strongly-Correlated Quantum Matter (Apr 6 - Jul 2, 2015). Online at <https://online.kitp.ucsb.edu/online/entangled15>; <https://online.kitp.ucsb.edu/online/entangled15/id.38>. May 2015.
- [14] Corinna Kollath, Andreas M. Läuchli, and Ehud Altman. “Quench Dynamics and Nonequilibrium Phase Diagram of the Bose-Hubbard Model”. In: *Phys. Rev. Lett.* 98 (18 Apr. 2007), p. 180601. DOI: [10.1103/PhysRevLett.98.180601](https://doi.org/10.1103/PhysRevLett.98.180601). URL: <https://link.aps.org/doi/10.1103/PhysRevLett.98.180601>.
- [15] Kevin A Landsman et al. “Verified quantum information scrambling”. In: *Nature* 567.7746 (2019), pp. 61–65.
- [16] Jun Li et al. “Measuring out-of-time-order correlators on a nuclear magnetic resonance quantum simulator”. In: *Physical Review X* 7.3 (2017), p. 031011.
- [17] Juan Maldacena. “The large-N limit of superconformal field theories and supergravity”. In: *International journal of theoretical physics* 38.4 (1999), pp. 1113–1133.
- [18] Juan Maldacena and Douglas Stanford. “Remarks on the sachdev-ye-kitaev model”. In: *Physical Review D* 94.10 (2016), p. 106002.
- [19] Goran Nakerst and Masudul Haque. “Chaos in the three-site Bose-Hubbard model: Classical versus quantum”. In: *Phys. Rev. E* 107 (2 Feb. 2023), p. 024210. DOI: [10.1103/PhysRevE.107.024210](https://doi.org/10.1103/PhysRevE.107.024210). URL: <https://link.aps.org/doi/10.1103/PhysRevE.107.024210>.

- [20] Daniel A Roberts and Brian Swingle. “Lieb-Robinson bound and the butterfly effect in quantum field theories”. In: *Physical review letters* 117.9 (2016), p. 091602.
- [21] Daniel A. Roberts and Brian Swingle. “Lieb-Robinson Bound and the Butterfly Effect in Quantum Field Theories”. In: *Phys. Rev. Lett.* 117 (9 Aug. 2016), p. 091602. DOI: [10.1103/PhysRevLett.117.091602](https://doi.org/10.1103/PhysRevLett.117.091602). URL: <https://link.aps.org/doi/10.1103/PhysRevLett.117.091602>.
- [22] Huitao Shen et al. “Out-of-time-order correlation at a quantum phase transition”. In: *Phys. Rev. B* 96 (5 Aug. 2017), p. 054503. DOI: [10.1103/PhysRevB.96.054503](https://doi.org/10.1103/PhysRevB.96.054503). URL: <https://link.aps.org/doi/10.1103/PhysRevB.96.054503>.
- [23] Stephen H Shenker and Douglas Stanford. “Black holes and the butterfly effect”. In: *Journal of High Energy Physics* 2014.3 (2014), pp. 1–25.
- [24] Brian Swingle et al. “Measuring the scrambling of quantum information”. In: *Phys. Rev. A* 94 (4 Oct. 2016), p. 040302. DOI: [10.1103/PhysRevA.94.040302](https://doi.org/10.1103/PhysRevA.94.040302). URL: <https://link.aps.org/doi/10.1103/PhysRevA.94.040302>.
- [25] Akram Touil and Sebastian Deffner. “Information Scrambling versus Decoherence—Two Competing Sinks for Entropy”. In: *PRX Quantum* 2 (1 Jan. 2021), p. 010306. DOI: [10.1103/PRXQuantum.2.010306](https://doi.org/10.1103/PRXQuantum.2.010306). URL: <https://link.aps.org/doi/10.1103/PRXQuantum.2.010306>.
- [26] Akram Touil and Sebastian Deffner. “Quantum scrambling and the growth of mutual information”. In: *Quantum Science and Technology* 5.3 (May 2020), p. 035005. DOI: [10.1088/2058-9565/ab8ebb](https://doi.org/10.1088/2058-9565/ab8ebb). URL: <https://dx.doi.org/10.1088/2058-9565/ab8ebb>.
- [27] Botao Wang and Ying Jiang. “Bogoliubov approach to superfluid-Bose glass phase transition of a disordered Bose-Hubbard model in weakly interacting regime”. In: *The European Physical Journal D* 70.12 (Dec. 2016). DOI: [10.1140/epjd/e2016-70459-y](https://doi.org/10.1140/epjd/e2016-70459-y). URL: <https://doi.org/10.1140%2Fepjd%2Fe2016-70459-y>.
- [28] Bin Yan, Lukasz Cincio, and Wojciech H. Zurek. “Information Scrambling and Loschmidt Echo”. In: *Phys. Rev. Lett.* 124 (16 Apr. 2020), p. 160603. DOI: [10.1103/PhysRevLett.124.160603](https://doi.org/10.1103/PhysRevLett.124.160603). URL: <https://link.aps.org/doi/10.1103/PhysRevLett.124.160603>.

- [29] Bin Yan and Wojciech H Zurek. “Decoherence factor as a convolution: an interplay between a Gaussian and an exponential coherence loss”. In: *New Journal of Physics* 24.11 (Nov. 2022), p. 113029. DOI: [10.1088/1367-2630/ac9fe8](https://doi.org/10.1088/1367-2630/ac9fe8). URL: <https://dx.doi.org/10.1088/1367-2630/ac9fe8>.
- [30] Norman Y Yao et al. “Interferometric approach to probing fast scrambling”. In: *arXiv preprint arXiv:1607.01801* (2016).
- [31] Beni Yoshida and Norman Y Yao. “Disentangling scrambling and decoherence via quantum teleportation”. In: *Physical Review X* 9.1 (2019), p. 011006.
- [32] Dong Yuan et al. “Quantum information scrambling in quantum many-body scarred systems”. In: *Phys. Rev. Res.* 4 (2 May 2022), p. 023095. DOI: [10.1103/PhysRevResearch.4.023095](https://doi.org/10.1103/PhysRevResearch.4.023095). URL: <https://link.aps.org/doi/10.1103/PhysRevResearch.4.023095>.
- [33] Qingling Zhu et al. “Observation of Thermalization and Information Scrambling in a Superconducting Quantum Processor”. In: *Phys. Rev. Lett.* 128 (16 Apr. 2022), p. 160502. DOI: [10.1103/PhysRevLett.128.160502](https://doi.org/10.1103/PhysRevLett.128.160502). URL: <https://link.aps.org/doi/10.1103/PhysRevLett.128.160502>.

# Appendix A

## Exponential of Matrix using Krylov subspace methods

The most time consuming part of the numerics we did to compute OTOC was to find the exponential of a matrix which is not diagonal in the conventional basis known to us. This is required to find out the time evolution operator which appears every time we evolve operators in the Heisenberg picture in the expression for OTOC. Since the size of Hilbert space for the Bose-Hubbard model scales exponentially with increase in number of sites, it becomes increasingly difficult and expensive to directly exponentiate the matrices. A number of methods are used to efficiently compute the exponential of a matrix and they include Krylov subspace methods . Pade approximation, the Chebyshev polynomials and other methods. Here, we use Krylov subspace methods in our work to setup a package in Julia that calculates the Out-of-Time Correlator for a given initial state of the system.

Given a matrix  $A$  and vector  $v$  , the Krylov subspace is given by:

$$\mathcal{K}_m(A, v) = \text{span}\{v, Av, A^2v, \dots, A^{m-1}v\}$$

where  $m$  is an integer. The orthogonal basis of this subspace  $\mathcal{K}_m(A, v)$  becomes the columns of a matrix  $V_m = [v_1, \dots, v_m]$  which is then a  $n \times m$  matrix.  $V_m$  is computed using Arnoldi

iteration and satisfies the following decomposition:

$$AV_m = V_{m+1}H_{m+1,m} \quad (\text{A.1})$$

where  $H_{m+1,m}$  is the known as the upper Hessenberg. Here, the entries of the matrix  $h_{i,j}$  are non-zero only if  $i \leq j + 1$ . Let  $H_{m,m}$  denote the matrix formed by the first  $m$  rows of  $H_{m+1,m}$ . Then, we can write Eq (A.1) as :

$$AV_m = V_m H_{m,m} + v_{m+1} h_{m+1,m} e_m^T \quad (\text{A.2})$$

$e_m = [0, \dots, 0, 1]^T \in \mathbb{R}^m$ . Eq (A.2) tells us that if you take any vector  $V_m$  from the Krylov subspace and multiply it with the matrix  $A$ , then we end up with a vector from the same subspace in addition to another term which is a multiple of the next basis vector in Krylov subspace  $v_{m+1}$ . Clearly, for this method to work, we would like the second term of Eq (A.2) to be small for some  $m$ .

Now, we intend to compute the action of the time evolution operator on a certain initial state. That is, we would like to compute  $y(t) = \exp(-tA)v$  for a given  $v \in \mathbb{R}^n$ . Once the basis for Krylov subspace and upper Hessenberg are found, we have the following approximation for  $y(t)$ :

$$y(t) = \exp(-tA)v = \exp(-tA)(V_m \beta e_1) \quad (\text{A.3})$$

$$\approx y_m(t) = V_m \exp(-tH_{n,m}) \beta e_1 = u_m(t) \quad (\text{A.4})$$

where  $\beta = \|v\|$ . Computing  $y_m(t)$  is much more affordable than  $y(t)$  when  $m \ll n$ . The iteration goes on based on the control defined over the following quantity:

$$r_m(t) = -Ay_m(t) - y_m'(t) \quad (\text{A.5})$$

It is easy to see that

$$\|r_m(t)\| = |h_{m+1,m} e_m^T u_m(t)| \quad (\text{A.6})$$

It might be the case that  $\|r_m(t)\| \approx 0$  for some specific points  $t$  only. So, ideally, one would like to compute something like the L2 norm  $\int_0^t \|r_m(s)\|^2 ds$ .

# Appendix B

## Bogoliubov transformation and the Bose-Hubbard Hamiltonian

Here, we show how the Bose-Hubbard model can be diagonalized only in certain limits of the coupling which is why we had to use Krylov subspace methods to compute the time evolution operator [27].

We start with the Bose-Hubbard Hamiltonian:

$$\begin{aligned} H &= -J \sum_{\langle i,j \rangle} a_i^\dagger a_j + \frac{U}{2} \sum_i n_i(n_i - 1) \\ &= -J \sum_{\langle i,j \rangle} a_i^\dagger a_j + \frac{U}{2} \sum_i a_i^\dagger a_i (a_i^\dagger a_i - 1) \\ &= -J \sum_{\langle i,j \rangle} a_i^\dagger a_j + \frac{U}{2} \sum_i a_i^\dagger a_i^\dagger a_i a_i \end{aligned} \tag{B.1}$$

Fourier transforming the operators using

$$a_i = \frac{1}{\sqrt{N}} \sum_k a_k e^{-ik \cdot x_i} \tag{B.2}$$

We can rewrite the Hamiltonian (B.1) for a hypercubic lattice of  $d$  dimensions as :

$$H = - \sum_k (2J \sum_{l=1}^d \cos ak_l) a_k^\dagger a_k + \frac{U}{2} \frac{1}{N} \sum_{k_1, k_2, k_3, k_4} a_{k_1}^\dagger a_{k_2}^\dagger a_{k_3} a_{k_4} \delta_{k_1+k_2, k_3+k_4} \quad (\text{B.3})$$

Note that the condition  $\delta_{k_1+k_2, k_3+k_4}$  implies that the corresponding term in the Hamiltonian is energy-conserving. The delta condition implies that  $k_1 + k_2 = k_3 + k_4$ . This condition can be rewritten as a bunch of other conditions as follows

1.  $k_1 + k_2 = 0$  and  $k_3 + k_4 = 0$
2.  $k_1 = 0 = k_2 = k_3 = k_4$
3.  $k_1 = k_3 (k_2 = k_4 = 0)$
4.  $k_1 + (k_2 = 0) = k_3 + k_4$
5.  $k_1 + k_2 = k_3 + k_4$

If we restrict ourselves to zero temperature or near-zero temperature, then it's fair to assume that the number of bosons with zero momentum  $N_0$  becomes macroscopically large. Then, we can write  $a_0 \approx a_0^\dagger \approx N_0$ . Using this, we rewrite the Fourier space Bose-Hubbard Hamiltonian as:

$$\begin{aligned} H = & (-2J \sum_{l=1}^d \cos a(k_l = 0)) a_0^\dagger a_0 - \sum_{k \neq 0} (2J \sum_{l=1}^d \cos ak_l) a_k^\dagger a_k \quad (\text{B.4}) \\ & + \frac{U}{2} \frac{1}{N} a_0^\dagger a_0^\dagger a_0 a_0 \text{ (Using condition 2)} + \frac{U}{2} \frac{1}{N} \sum_{k \neq 0} a_k^\dagger a_{-k}^\dagger a_0 a_0 \text{ (Using condition 1)} \\ & + \frac{U}{2} \frac{1}{N} \sum_{k \neq 0} a_0^\dagger a_0^\dagger a_k a_{-k} \text{ (Using condition 1)} + \frac{U}{2} \frac{1}{N} \sum_{k \neq 0} a_k^\dagger a_0^\dagger a_k a_0 \text{ (Using condition 3)} \\ & + \frac{U}{2} \frac{1}{N} \sum_{k_1, k_2 \neq 0} a_{k_1}^\dagger a_{-k_1}^\dagger a_{k_2} a_{-k_2} \text{ (Using condition 1)} \end{aligned}$$

We now invoke the weak coupling approximation where we only retain terms which are upto second order in  $a_k/a_k^\dagger$ , this is when  $U < J$ . This is why we did not consider Condition



4 and 5 while expanding the Hamiltonian in Eq (B.4) and using the same logic, we also choose to ignore the last term in Eq (B.4). Now substituting  $a_0 \approx a_0^\dagger \approx N_0$  and after a little rearrangement, we get

$$H = \frac{U}{2}(n_0 - 2dJ)N_0 - \sum_{k \neq 0} \left( \frac{U}{2}n_0 - 2J \sum_{l=1}^d \cos ak_l \right) a_k^\dagger a_k + \frac{U}{2}n_0 \sum_{k \neq 0} (a_k^\dagger a_{-k}^\dagger + a_k a_{-k}) \quad (\text{B.5})$$

Renaming a few terms, we arrive at the Hamiltonian

$$H = \frac{U}{2}(n_0 - 2dJ)N_0 - \sum_{k \neq 0} A_k a_k^\dagger a_k + \frac{U}{2}n_0 \sum_{k \neq 0} (a_k^\dagger a_{-k}^\dagger + a_k a_{-k}) \quad (\text{B.6})$$

where

$$A_k = \frac{U}{2}n_0 - 2J \sum_{l=1}^d \cos ak_l \quad (\text{B.7})$$

and  $n_0 = N_0/N$  is the particle density with zero momentum. Clearly, Eq (B.6) is in the form where we can apply the Bogoliubov transformation which results in the following diagonalized Hamiltonian

$$H = \left( \frac{Un_0}{2} - 2dJ \right) N_0 + \frac{1}{2} \sum_{k \neq 0} (E_k - A_k) + \sum_{k \neq 0} E_k b_k^\dagger b_k \quad (\text{B.8})$$

where

$$E_k = \sqrt{A_k^2 - (Un_0)^2} \quad (\text{B.9})$$

and

$$u_k^2 = \frac{1}{2} \left( \frac{A_k}{E_k} - 1 \right), v_k^2 = \frac{1}{2} \left( \frac{A_k}{E_k} + 1 \right) \quad (\text{B.10})$$

Hence, the new Hamiltonian (B.8) is diagonal in the Bogoliubov transformed operators  $b_k, b_k^\dagger$ . But this was only possible under the condition that  $U < J$ . This means even when the coupling strength is weak, we have to throw away high order energy-conserving terms to diagonalize the Hamiltonian analytically. Hence, this analytic approach is not optimal to explore the Bose Hubbard model at the coupling strengths considered in this thesis to compute the OTOC because in the strong coupling limit, as also mentioned in the section on Bose-Hubbard model, it is these higher order quartic interaction terms that are responsible for thermalization in Bose-Hubbard model and in this very limit, we find the system to be quantum chaotic and the OTOC is characterised by a Gaussian to exponential transition.